Long-term evolution of a carbonate reservoir submitted to fresh, saline and thermal waters interactions – Jurassic carbonates in the coastal area of the Gulf of Lion margin (southern France)

Florian Widhen, Michel Séranne, Grégory Ballas, Pierre Labaume, Erwan Le-Ber, Philippe Pezard, Flavia Girard, Claudine Lamotte, Bernard Ladouche

BSGF - Earth Sciences Bulletin 2023, 194, 7
© F. Widhen *et al.*, Published by EDP Sciences 2023
https://doi.org/10.1051/bsgf/2023005

BSGF
Earth Sciences Bulletin
Available online at:
www.bsgf.fr

Open Access

Long-term evolution of a carbonate reservoir submitted to fresh, saline and thermal waters interactions – Jurassic carbonates in the coastal area of the Gulf of Lion margin (southern France)

Florian Widhen[1], Michel Séranne[1,*], Grégory Ballas[1], Pierre Labaume[1], Erwan Le-Ber[1], Philippe Pezard[1], Flavia Girard[1], Claudine Lamotte[2] and Bernard Ladouche[2]

[1] Géosciences Montpellier, Université de Montpellier–CNRS, Montpellier, France
[2] BRGM, Montpellier, France

Received: 4 May 2022 / Accepted: 27 March 2023 / Publishing online: 4 May 2023

Abstract – Securing and managing underground water resources requires a good knowledge of the structure, texture and connections of the reservoir, in order to develop realistic and reliable hydrogeological models. On the coastline of the Gulf of Lion Margin (S. France), the Balaruc-les-Bains deep karst reservoir is subjected to interactions between fresh, marine and deep thermal waters, respectively. Water resource usage for drinking, spa resort, and fish-farming raises important economic and social issues. These were addressed by an integrated research program, involving drilling of an exploratory borehole across the Jurassic carbonate reservoir. This contribution analyses the 750 m cores, in order to (i) characterise the architecture and evolution of the karst reservoir and (ii) investigate the paleo-fluids circulations, witnessed by calcite and dolomite mineralization in the fractures, karst cavities, and as cement of tectonic beccia. The structure of the reservoir is characterised by the superposition of several aquifers separated by marly intervals. At shallow level, the initial grainstone is incompletely dolomitized in metre-thick intervals, while limestone in the 210–340 m interval was completely dolomitized at an early stage. Dolomite has been subjected to penetrative extensional cataclastic deformation, while the preserved limestone is affected by normal faulting, resulting from NNE–SSW extension. Distinct types of karsts have been documented, from the top of the reservoir (paleo-lapiaz filled with Burdigalian marine marls), down to 500 m depth (paleo-endokarst filled with continental silts). The upper reservoir (75–150 m) is intensely karstified, and includes 0.1 to 1 m-wide cavities, where present day water fluxes are documented. Analyses of calcite and dolomite crystallisation under natural light and cathodoluminescence indicate precipitation from distinct fluids: formation water in chemical equilibrium with the host rock, water rich in oxides and hydroxides, ascending hydrothermal fluid and corrosive water of meteoric origin. Alternate dolomitization and calcitization observed in the upper reservoir suggests alternate flows of karstic freshwater and marine salt-water. Vertical, metre-long and centimetre wide open cracks are presently used for large water flows; several generations of syntaxial calcite growth provide evidence for varying chemistry of the circulating fluids. Structural cross cutting relationships allowed us to establish a relative chronology of events, which can be correlated with the regional geodynamic evolution. The study reveals that the present-day reservoir architecture results from the superimposition of structures formed during the Early Cretaceous extension, Maastrichtian-Eocene Pyrenean shortening, and Oligocene rifting of the Gulf of Lion. The reservoir was also shaped by successive karstification episodes and marine transgressions. Although the present-day hydrological system is controlled by, and reactivates structures inherited from a long-term evolution, it is characterised by frequent turn-overs of the water flow, tuned by high-frequency external forcings such as sea-level changes driven by Pleistocene glacio-eustasy, or varying precipitation rates.

Keywords: carbonate reservoir / aquifer / karst / calcite veins / thermal water / marine water

*Corresponding author: michel.seranne@umontpellier.fr

Résumé – Évolution long terme d'un réservoir carbonaté soumis à des interactions entre eaux douces, salines et thermales : les carbonates du Jurassique de la zone côtière de la marge du Golfe du Lion (sud de la France). L'approvisionnement et la gestion des eaux souterraines nécessitent une bonne connaissance de la structure, de la texture et des connexions des réservoirs géologiques, afin de développer des modèles hydrogéologiques utilisables et réalistes. Le réservoir karstique profond de Balaruc-les-Bains, situé sur la côte du Golfe du Lion, est soumis à des interactions entre eaux douces, eaux marines et eaux thermales profondes. La gestion des différentes ressources en eau, pour l'alimentation, les thermes et la pisciculture/ostréiculture, constitue d'importants enjeux économiques et sociétaux pour le territoire. Ceux-ci sont abordés dans le cadre d'un programme de recherche impliquant le forage d'un puits carotté d'exploration, dans le réservoir carbonaté du Jurassique. Cette contribution analyse les 750 m de carotte recueillis, afin de (i) caractériser l'architecture et l'évolution du réservoir karstique et (ii) investiguer les paléocirculations de fluides dont témoignent les cristallisations de calcite et dolomite dans les fractures, les cavités karstiques et comme ciment de brèches tectoniques. La structure du réservoir se caractérise par la superposition de plusieurs aquifères séparés par des intervalles marneux. À faible profondeur, le grainstone initial est incomplètement dolomitisé sur des niveaux métriques, alors que le mudstone de l'intervalle 210–340 m est totalement dolomitisé. La dolomie est affectée par une déformation pénétrative, extensive, cataclastique, alors que le calcaire préservé est affecté par des failles normales. L'ensemble résulte d'une extension NNE–SSW. Plusieurs types de karst sont distingués, depuis le sommet du réservoir (paléo-lapiaz remplis de marnes marines du Burdigalien), jusqu'à plus de 500 m de profondeur (paléo-endokarsts remplis de silts d'origine continentale). Le réservoir supérieur est intensément karstifié, présentant des cavités décimétriques à métriques dans lesquelles d'importantes circulations actuelles d'eau ont été mises en évidence. L'observation des cristallisations de calcite et dolomite en lumière naturelle et en cathodoluminescence indique des précipitations à partir de fluides distincts : des eaux de formation en équilibre avec la roche encaissante, des eaux chargée en oxydes et hydroxydes, des fluides hydrothermaux ascendants, et des eaux corrosives d'origine météorique. Des alternances de dolomitisation et de calcitisation observées dans le réservoir supérieur suggèrent des flux alternés d'eaux salées marines et d'eaux douces karstiques. Des fentes verticales ouvertes, d'extension métrique et de largeur centimétrique, permettent des flux importants d'eau ; plusieurs générations de croissance syntaxiale de calcite montrent une évolution de la chimie du fluide qui y circule. Les relations structurales entre les veines permettent d'établir une chronologie relative des évènements, qui est corrélée avec l'évolution géodynamique régionale. Cette étude montre que l'architecte actuelle du réservoir résulte de la superposition de structures formées pendant : l'extension néocomienne, le raccourcissement Pyrénéen entre le Maastrichtien et l'Éocène, et le rifting du Golfe du Lion pendant l'Oligocène. Le réservoir a également été affecté par une succession d'épisodes de karstification et de transgressions marines. Bien que contrôlé par des structures héritées d'une évolution géodynamique sur le long terme, le système hydrologique actuel est caractérisé par de fréquentes inversions des flux hydriques, modulées par des forçages externes de (très) haute-fréquence, tels que les variations du niveau de la mer résultant du glacio-eustatisme pendant le Pléistocène ou des variations du régime de précipitation.

Mots clés : réservoir carbonaté / aquifère / karst / veines de calcite / eau thermale / eau marine

1 Introduction

Securing water resources is currently a major challenge, especially in the semi-arid to arid Mediterranean countries where population and economic development concentrate along the coastline. In southern France, excessive use of underground water resources may lead to seawater intrusion and salinisation of sedimentary coastal aquifers (Petelet-Giraud *et al.*, 2016; de Montety *et al.*, 2008). In the case of coastal karst aquifers, salinisation may also occur, by direct seawater inflow in the karst at surface (Drogue and Bidaux, 1986; Arfib and Gilli, 2010) or at depth through inherited karst network (Fleury *et al.*, 2007; Gilli, 2020). Alternatively, or additionally, salinisation of coastal karst aquifers may result from mixing surface waters with fossil seawater, trapped in the reservoir (Khaska *et al.*, 2013). It may also reflect interaction with deep saline thermal waters (Khaska *et al.*, 2015). The interaction of a significant proportion (several percent) of deep brines with shallow karst freshwater is commonly described in karstic reservoirs (Bicalho *et al.*, 2019). Also, upflow of fluids from deep reservoirs may bring warmer geothermal waters in the near-surface karstic reservoirs (Cantarero *et al.*, 2013; Petrini *et al.*, 2013).

Mixing processes between chemically and thermally distinct fluids depends on the geological structure and texture of reservoirs. In tectonically complex and polyphase areas, it is pivotal to consider the 3D position of the segmented parts of the reservoir offset by faults, to understand and model hydrological systems (*e.g.* Husson *et al.*, 2018).

The geological evolution of the reservoir, which involves processes such as sedimentation, subsidence, uplift, weathering and deformation, spans tens to hundreds of millions of years and controls the present-day hydrogeological setting. However, the hosted hydrological system, which depends on parameters such as sea-level change or amount of precipitation, is varying on much shorter time scales (10^4 to 10^5 years). Consequently, interactions between the long-term evolution of

the reservoir structure and the short-term evolution of the hydrological system may induce periodic or temporary changes, and cumulative effects, while only the present-day hydrological system can be monitored.

The signature of past interactions between host-rock and fluids can be sought in the mineralization. Cross-cutting relationships of successive generations of veins provide a relative chronology (Cantarero *et al.*, 2013). Developments of U-Pb dating of calcite filling veins (Roberts and Walker, 2016; Hansman *et al.*, 2018) open new perspectives on absolute dating of tectonic events (Beaudoin *et al.*, 2018; Parizot *et al.*, 2021) and help reconstructing the evolution of paleo-hydrological systems (Pagel *et al.*, 2018; Yang *et al.*, 2022). This could help reconstructing the evolution of the paleo-hydrosystems.

Balaruc-les-Bains is the largest spa town in France (more than 50,000 visitors annually). It is located along the shoreline of the Gulf of Lion margin (NW Mediterranean), where Neogene post-rift marls onlap the inherited Mesozoic carbonate platform, along a complex topography that includes carbonate promontories, lagunas and low-land alluvial plains (Fig. 1). Underground hydrology of the area (Aquilina *et al.*, 2002; Pétré *et al.*, 2020 and references therein) is characterised by the interaction of: (i) karstic freshwaters recycled from precipitations over the carbonate plateaus hinterland, (ii) marine and brackish waters percolating from the Mediterranean Sea and the Thau Laguna, respectively, and (iii) hydrothermal hot waters ascending from a deep reservoir. Water management must address the balance between: (i) supplying drinking water for a large population, which increases with summer tourism during the drought summer period, and (ii) preserving the quality of the hydrothermal water for the spa.

The overall objective of the Dem'Eaux Thau Project, which encompasses the present study, is to qualify and quantify the interactions of the different waters in the karst reservoir to improve water(s) management (Ladouche *et al.*, 2019). An exploration well was drilled down to 750 m deep in the Jurassic carbonate reservoir in order to investigate the structure and the hydrological setting of the deep reservoir. The objective of the present contribution is to presents the preliminary results of the structural study of the 750 m long core sampled along the borehole. Core visual and microscopic analyses allowed to determine the structure of the reservoir and to understand the different post-depositional deformation, alterations and paleofluid circulations. Correlation of the successive events determined from the core analyses with the geodynamic evolution of the area helps to reconstructing the long-term geological evolution of the reservoir.

2 Geological and hydrogeological context

The studied karstic reservoir results from a polyphase tectonic evolution starting with the deposition of marine carbonates and marls on the NW Tethys margin, during the Jurassic and Valanginian (Debrand-Passard and Courbouleix, 1984). Bathonian to present formations are exposed in the Thau watershed (Gottis *et al.*, 1967). The continuous Mesozoic marine sedimentation on the Tethys margin stopped during the middle part of the Cretaceous, as a result of uplift, erosion and weathering in continental environment, and led to the development of (i) a remarkable regional unconformity and (ii) bauxites formation (Combes, 1990). The latter was trapped in the karstified carbonates of Late Jurassic age, which makes a distinctive geodynamic marker across the study area (Lajoinie and Laville, 1979) (Fig. 1). This episode known as the "Durancian Uplift" (Gignoux, 1926) was recently dated in the study area to Albian (Marchand *et al.*, 2020). It is related to the late Early Cretaceous rifting of the Pyrenean domain (Lagabrielle *et al.*, 2010; Duretz *et al.*, 2020) and offshore Provence domain (Fournier *et al.*, 2016), both located south of the study area. Symmetrically, the Durancian Uplift is also related to the kilometre-scale uplift of the hinterland, as rift shoulders (Barbarand *et al.*, 2001; Marchand *et al.*, 2020) in the Massif Central, north and northwest of the study area.

Later, the area underwent Pyrenean NS shortening, during Maastrichtian to Eocene times (Arthaud and Séguret, 1981; Arthaud and Laurent, 1995). The Pyrenean shortening is characterised by folding and thrusting of the Mesozoic carbonate cover, above Triassic detritals and evaporites decollement (Hemelsdaël *et al.*, 2021b) (Fig. 1). Finally, the area recorded the Chattian–Aquitanian rifting of the Gulf of Lion margin, characterised by NW–SE extension producing half-grabens bounded by NE-trending normal faults, and filled by continental syntectonic breccia and marls (Benedicto *et al.*, 1996; Benedicto *et al.*, 1999). The study area does not expose synrift basins, but it is partly covered by post-rift Burdigalian marine sediments that onlap paleo-reliefs. The latter correspond to the hanging-walls of the previous Pyrenean thrusts (Hemelsdaël *et al.*, 2021b). Post-rift sequence thickens offshore (to the SE) in the direction of increasing thermal subsidence following the opening of the Ligurian-Provencal oceanic back-arc basin (Séranne, 1999). The post-rift sequence is truncated by the Messinian erosional surface (MES), which developed in response to the desiccation-related drop of the Mediterranean sea-level (Clauzon, 1973). During the Messinian, the hydrological network adapted to the large scale base-level drop (1000 m) by: (i) incision of the detrital Cenozoic sediments (Clauzon, 1982) and (ii) deep karstic incision in the Mesozoic carbonates (Audra *et al.*, 2004). The MES is observed onshore in the study area (Ambert *et al.*, 1998) and it is filled by the Pliocene to Pleistocene progradational prism, made of marine clays, littoral to alluvial-plain marls and sandstones (Fuchey *et al.*, 2001; Lofi *et al.*, 2011). The Pliocene sequences present similar hydrologic properties than the underlying Burdigalian interval, *i.e.* both marl-dominated formations act as a seal for the underlying karstified Jurassic carbonates.

The hydrogeological setting is characterised by three distinct underground waters converging towards the studied Jurassic reservoir (Fig. 2) (Bérard, 1995; Ladouche *et al.*, 2001; Aquilina *et al.*, 2002; Aquilina *et al.*, 2003; Pétré *et al.*, 2020):

– the karstic, cold, fresh waters are fed by rain on the Jurassic hills and plateaus making a circa 200 km^2 recharge area (Causse d'Aumelas, Fig. 1). The NS-oriented underground karst network has been traced along several resurgences and the Vise spring is the downstream-most resurgence, located in the Thau laguna at 30 m deep. There, freshwater flows at an average flux of 110 l/s (Ladouche *et al.*, 2021) into the brackish waters of the laguna;

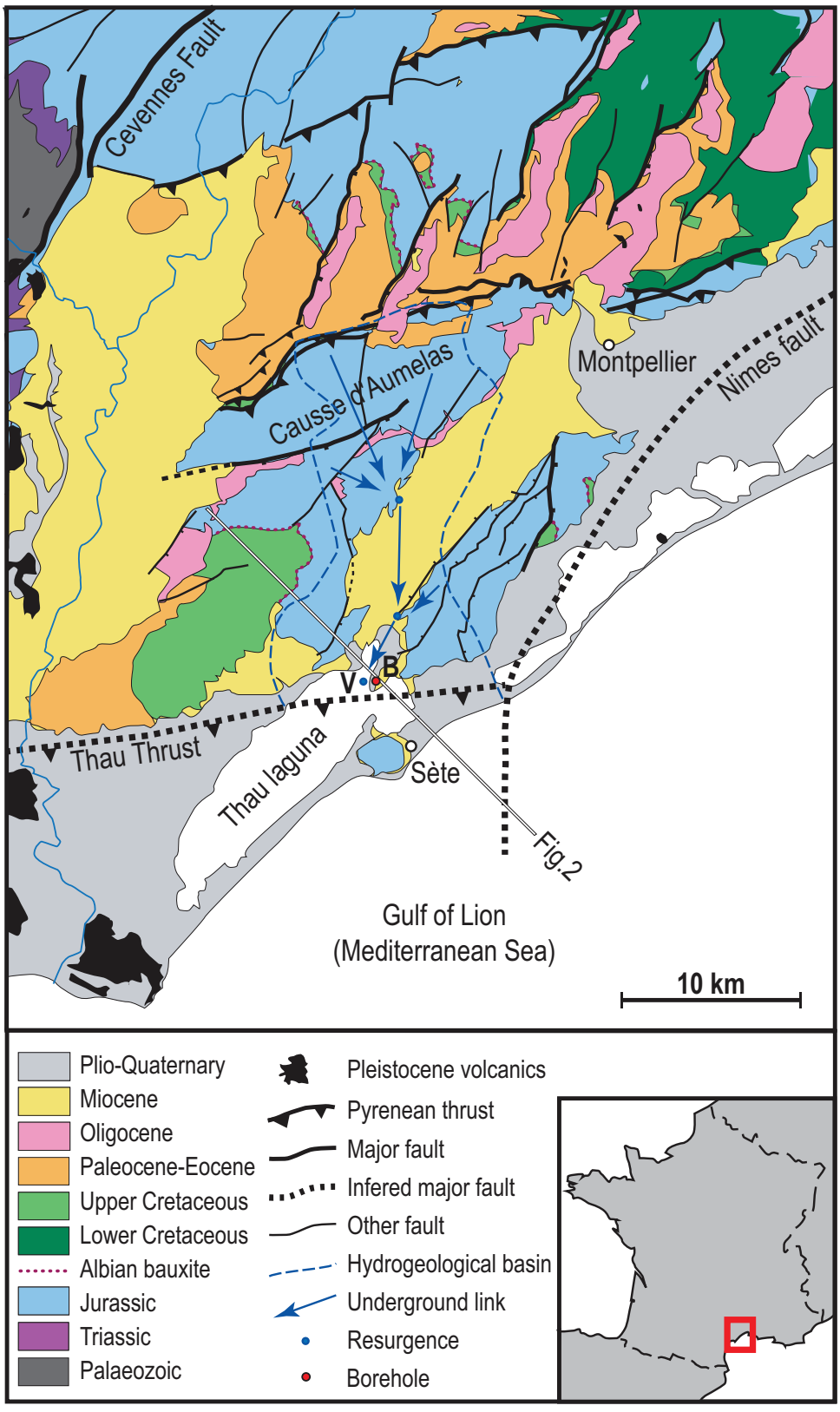

Fig. 1. Geological map of the study area (modified from Hemelsdaël *et al.*, 2021b). B: Balaruc-les-Bains; V: submarine Vise spring.

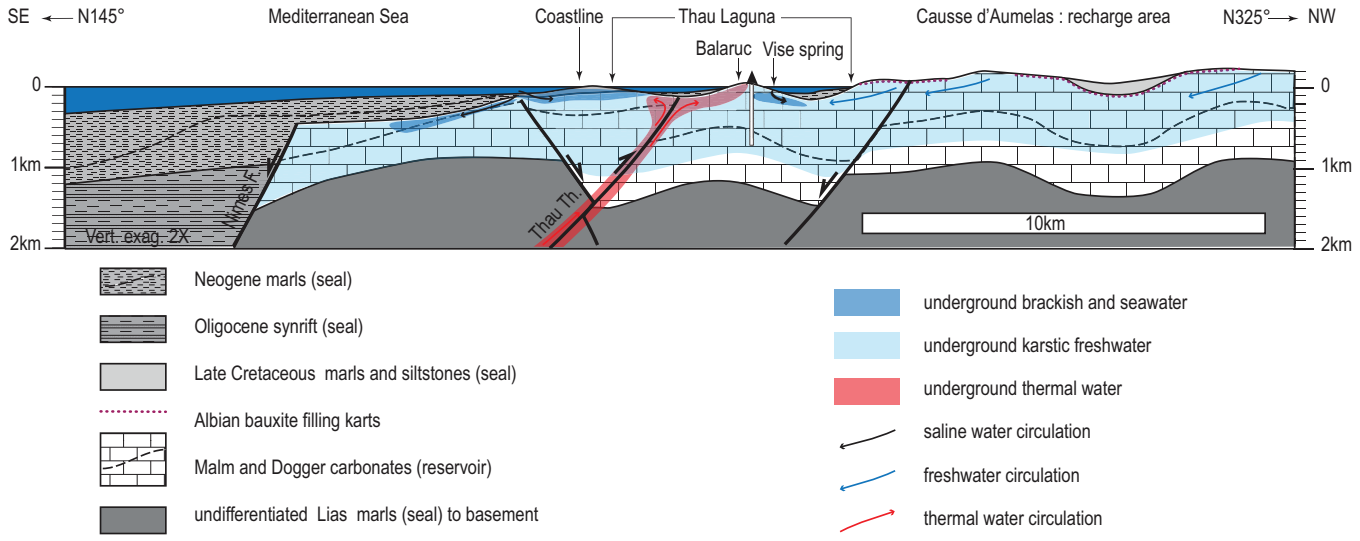

Fig. 2. Simplified geological section across the study area highlighting the hydrological system. Position of the section is indicated on Figure 1.

– the carbonate reservoir can be intruded by saltwater wedge (Pinault *et al.*, 2004), especially along the southeastern shoreline (Drogue and Bidaux, 1986). Remarkably, during specific time intervals, the Vise spring absorbs brackish waters, with downward fluxes that may exceed 300 l/s (Ladouche *et al.*, 2021). This reversal, locally known as "inversac" (Gèze, 1987) has been documented seven times since the middle of the XXth century (Bérard, 1995) and has been continuously monitored since 2018 (flow, temperature, electrical conductivity, pressure, and chemistry; Lamotte, 2019). This new equipment allowed to accurately record the last "inversac" that started in November 2020 and stopped in March 2022. No periodicity or specific duration of the phenomenon has been evidenced. The documented reversals of flow occurred during periods of low freshwater piezometric level in the underground reservoir, whether it was natural (pluriannual drought periods) or artificial (*e.g.* pumping in neighbouring mines; Pétré *et al.*, 2020);
– the third fluid consists in the saline thermal waters (30–50 °C) that are exploited at Balaruc-les-Bains spa. Historically, thermal waters were naturally flowing from a spring, but it was later pumped from the top of the carbonate reservoir sealed by the Neogene marly sediments, through a series of production wells. Hydrogeochemistry suggests that thermal fluids are interacting with shallow meteoric water (Aquilina *et al.*, 2002) and that the "pure" thermal end-member is a mixture of seawater and meteoric paleo-waters (Aquilina *et al.*, 2002). Thermal waters are rising up from a deep reservoir, through a major reverse fault: the Thau Thrust (Figs. 1 and 2) (Pétré *et al.*, 2020; Hemelsdaël *et al.*, 2021b).

3 Material and methods

3.1 Boreholes

This contribution relies on a group of 4 vertical boreholes drilled from a single 10 × 10 m platform in Balaruc-les-Bains. Wells #1 and #2 were bored by destructive drilling (45 m and 170 m depth, respectively) and were used for testing the hydrological behaviour of shallow reservoirs. Well #3 was drilled and entirely cored from the surface down to 300 m. Well #4, designed to explore the deepest part of the reservoirs, was bored at 3 m distance of well #3 by destructive drilling down to 290 m, then cored from 290 m down to 750 m depth. Considering the short distance between wells #3 an #4 and the 10 m overlap of the cores, which allowed accurate correlation, the two cored wells are integrated within one synthetic log, and interpreted as a single borehole from surface down to 750 m depth. Drilling was lubricated, and cuttings were extracted, with mud. Extra water outflows were recorded at the wellhead and interpreted as a result of the borehole cross-cutting a water vein.

3.2 Cores

Cores diameters are 85 mm and 61 mm in the 0–200 m and the 200 m to bottom intervals, respectively. Cores are not oriented with respect to the North; the vertical cores display a very low dipping stratification plane, in agreement with the $<10°$ dip observed in neighbouring outcrops. Examination of the cores took place on the site, where a high-resolution 1/100-scale log was measured.

Sedimentary petrology and sedimentology were analysed (Fig. 3). However, the cores of the upper 400 m are characterised by an unsuspected amount of deformation, which often prevents classical diagnostic sedimentological observations. Two distinct deformation styles are identified: (i) penetrative brecciation displaying metre-wide strain gradient, (ii) discrete faulting; cores being naturally cut along the fault plane allow observation of the slickensides, which consistently indicate a normal sense of motion. Fractures, stylolites and veins are also analysed and recorded. Finally, macroscopic analyses of the cores allow record of alteration features and specifically karstification, with special attention to karst cavities infill.

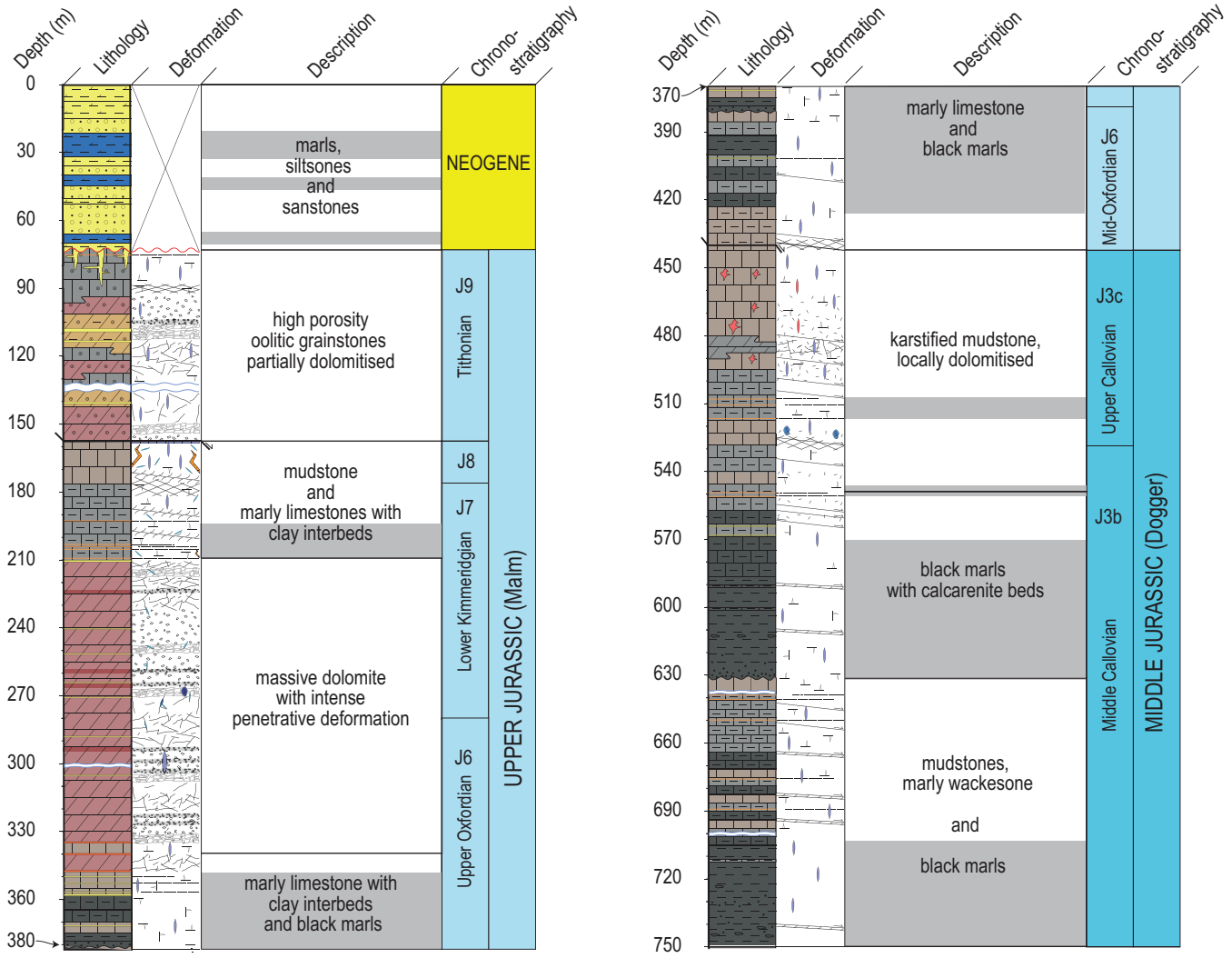

Fig. 3a. Synthetic lithostratigraphic and deformation log of the Balaruc-les-Bains drill core (left column).

3.3 Optical Borehole Imager

A series of logging tools were used in the borehole, however, this contribution focuses only on Optical Borehole Imager (OBI) (Gaillot *et al.*, 2005; Gaillot *et al.*, 2007) as a mean to orientate the structures. Indeed, optical images of the borehole acquired by OBI, which is associated with a magnetometer, displays planar structures as sinusoides. The amplitude of the sinusoid reflects the dip (knowing the borehole diameter), while the maxima and minima provide orientation with respect to the magnetic North. High quality optical imaging allows to correlate the sinusoids from OBI with the structures observed on cores (Fig. 4) where the sense of motion can be determined by direct observation of the slickensides. It was thus possible to analyse the kinematics of structures and discuss the orientation of the stresses that generated them. Well #3 was imaged from 101 m to 298 m and well #4 was imaged from 310 m to 750 m. Unfortunately, the 298–310 m interval could not be imaged.

3.4 Optical microscopy

Standard and polished thin-sections of core samples (100 mm thick) were examined under plane polarized light without impregnation. Classical optical microscopy with an Olympus BH2 microscope supported sedimentological and microstructural analyses.

3.5 Cathodoluminescence

Cathodoluminescence (CL) of calcite or dolomite crystals was used to investigate carbonate cements stratigraphy. Colors and intensities are commonly correlated with Mn^{2+} and Fe^{2+} content. It has been argued that high concentrations of Mn^{2+} activates luminescence, whereas concentrations of 1 to 1.5 wt% Fe^{2+} inhibits luminescence of calcite (Richter *et al.*, 2003), although this usually need to be confirmed with additional geochemical data (Machel, 2000). In his

b : LEGEND

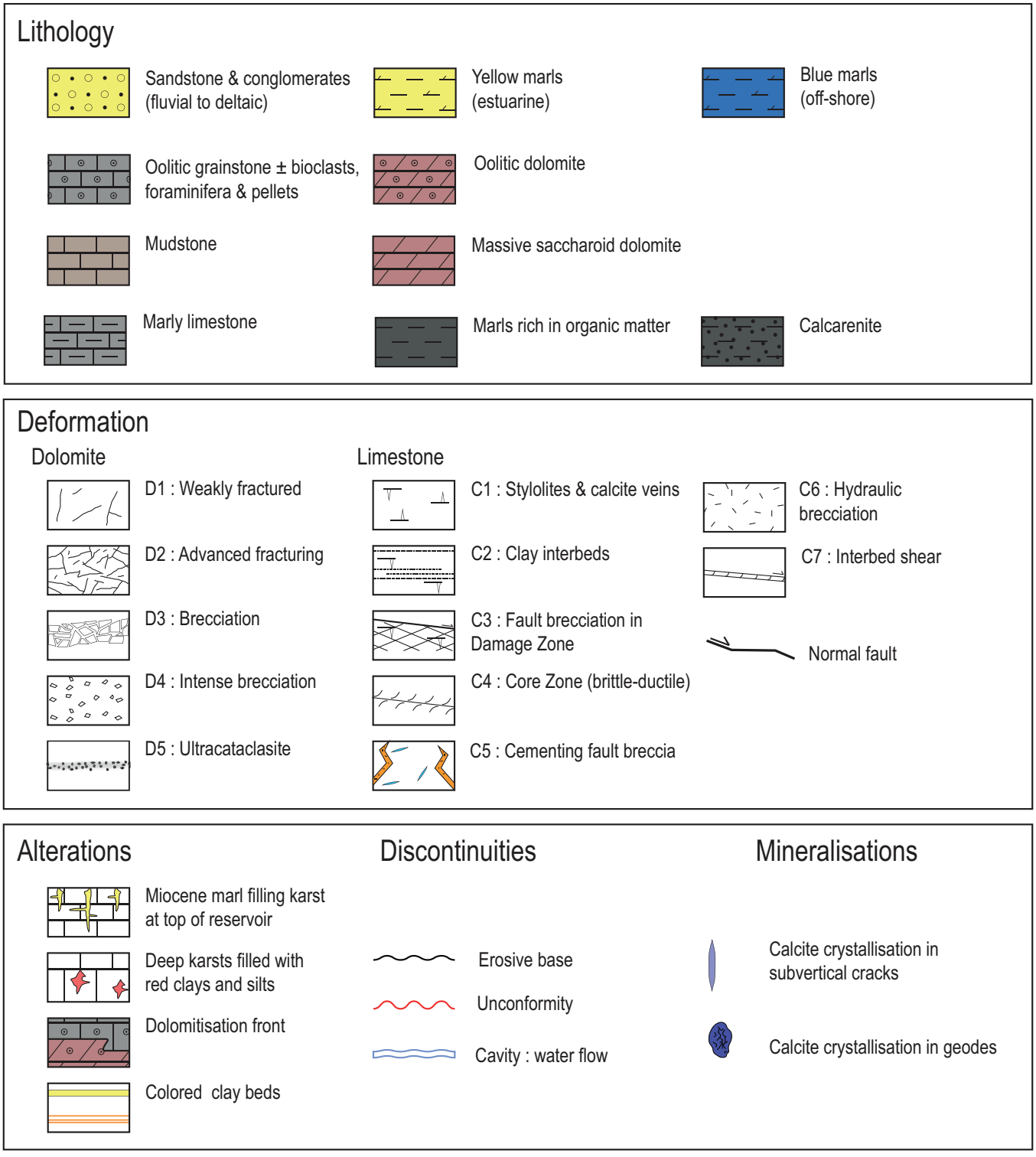

Fig. 3b. Detailed legend of the logs.

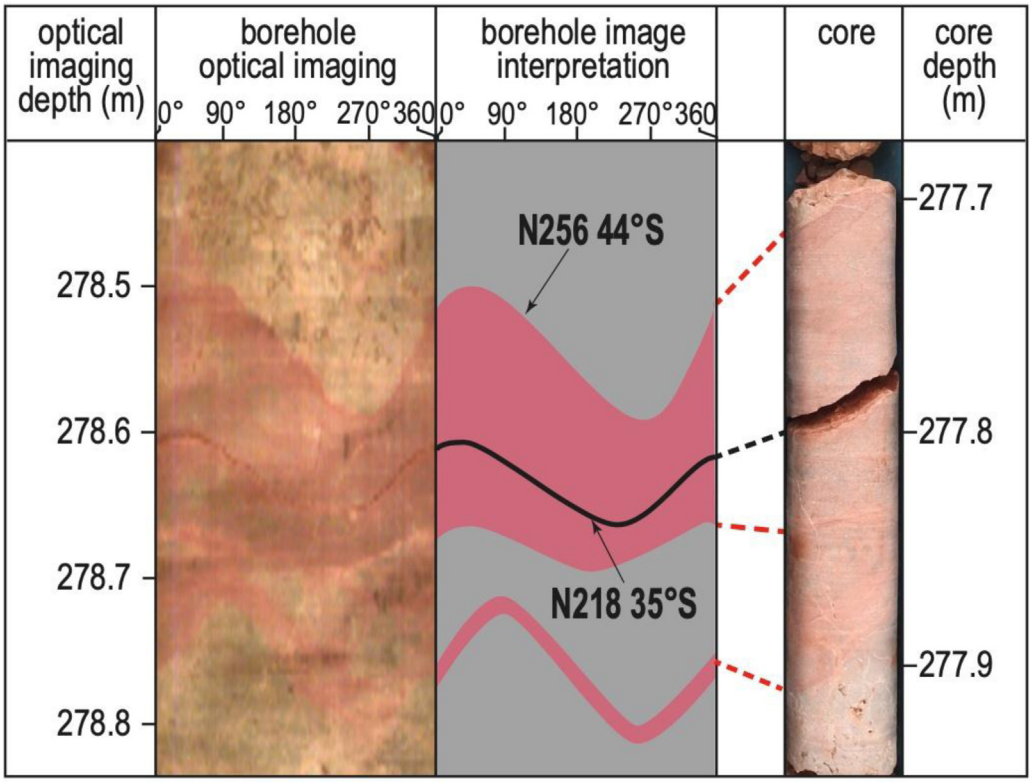

Fig. 4. Different facies of deformation observed in cores of limestone lithology: a: compaction related stylolithes and associated extension calcite veins in mudstones; b: in marly limestones; c: brecciated limestones in fault damage zone, note mudstones and clasts of calcite vein; d: intense deformation in fault core zone characterised by centimetre-scale extensional shear-zones (arrows) affecting both stylolitized limestones and veins; note the genetic relationship between bedding-parallel stylolites and sub-vertical calcite veins in the poorly deformed host limestone; e: hydraulic breccia sealed by calcite; note the late vertical fractures, partially cemented.

preliminary study, CL was used to distinguish different generations of crystal growths and cements; it also provided qualitative clues on the chemistry of the crystals. A CITL cold cathodoluminescence model Mk5, operating with a vacuum of 0.035 mBar, a tension of 14 kV and current intensity of 250 mA was employed. Observations were made with an Olympus BX41 microscope and a Diagnostic Instruments Spot RTKE 7.3 camera.

3.6 Back Scattered Electron imaging

Back Scattered Electron (BSE) imaging was acquired at the MEA platform of the University of Montpellier, using a HitaschiS-2600N equipment. BSE imaging allowed analyses of deformation mechanisms and distinction of carbonate minerals. The latter was confirmed with qualitative elements maps generated by Energy Dispersive X-ray Spectrometry (EDS).

4 Structure of the reservoir

4.1 Lithostratigraphy

The lateral extent of the reservoir is controlled by integrating surface geology, seismic reflection, passive seismic imaging and gravimetry interpretations (Hemelsdaël *et al.*, 2021a; Hemelsdaël *et al.*, 2021b), and hydrogeological tracing and monitoring (Ladouche *et al.*, 2019; Pétré *et al.*, 2020). The 3 m apart boreholes #3 and #4 have been entirely cored, allowing the high resolution lithostratigraphic and structural analyses of one synthetic well-record presented here, from top to bottom (Fig. 3).

In the Balaruc area, the Jurassic karstic reservoir is covered by a 74 m thick Miocene sequence made of marine marl, interbedded with coarse to medium sandstone, and topped by several metres of Pliocene fluvial conglomerates. Although the Miocene conglomerate and sandstone contain an aquifer, the whole Mio-Pliocene interval acts as a non-permeable cover for the underlying limestone.

From 74 to 157 m, the borehole samples the Tithonian carbonates dipping about 10° to the NE. The top is affected by karstification displaying small-cale lapiaz filled with the overlying Miocene marls. These distinctive yellow marls are present in karstified fractures down to 90 m depth. The cores display a complex succession of light-grey oolitic grainstones interbedded with dolomitized intervals, which are characterised by a reddish, high-porosity, crumbly material, and presence of centimetre-size dissolution cavities. Several discontinuities in the core-record correspond to karstic cavities, correlated with water flows encountered during drilling. The major one (1.7 m hollow) is located at around 135 m depth. The base of this interval corresponds to an

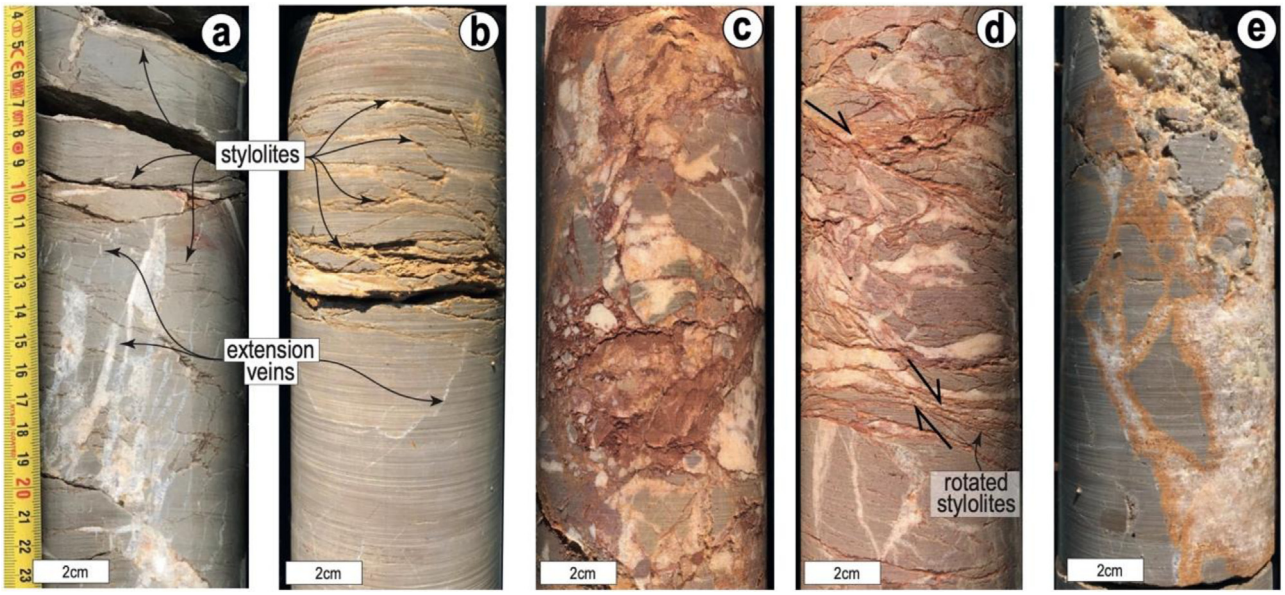

Fig. 5. Gradient of deformation observed in the dolomite facies, increasing from left (a) to right (e). The top panel shows the structures observed on cores, the middle panel provides illustrations of fracturing and cataclasis, observed under optical microscope in plane-polarized light; the lower panel gives example of microstructures on SEM images that give evidence for cataclasis by fracturing the dolomite along the crystals twinnings (white arrows).

extensional fault cutting the dolomite, revealed by a striated plane.

From 157 to 210 m, below the normal fault, the lithology consists of thick massive beds of grey-beige mudstone of Upper Kimmeridgian age, dated by correlation with surface exposure. The lithostratigraphic change on each side of the fault argues for several tens of metres offset across the fault. Below the mudstone, occurs a thicker interval of brown marly limestone, the basal part of which presents clayey interbeds up to 4 cm thick.

From 210 to 345 m, extends a circa 135 m thick, reddish, entirely dolomitized, interval. Up to 6 fine clay levels represent the marly interbeds of the original limestone. A distinctive feature is the penetrative brittle deformation that affects the whole interval, although with varying intensity (see below). At around 300 m depth, a major water flow has been recorded during drilling. Although no direct stratigraphic evidence could be found in the cores, its position below the upper Kimmeridgian suggests that this interval covers the Lower Kimmeridgian to the Upper Oxfordian.

From 345 to 440 m, are found alternating 5–10 m-thick beige to grey marly fossiliferous limestones and dark to black marls. The base is marked by a minor fault zone. This interval of Oxfordian age is classically considered as an low-permeability unit (Dörfliger *et al.*, 2008).

From 440 to 550 m, a massive beige mudstone displays 2 to 5 cm large karstic cavities, completely filled up with red siltstone. In the following, we name karst or karstic cavities, centimetre- to metre-size cavities that result from dissolution of lithified carbonate. This mudstone shows intense fracturing with calcite mineralization filling the fractures. It is locally dolomitized and it overlies marly limestones with thin clayey interbeds. This interval is of Upper Callovian age. When exposed in outcrop, the Lower Oxfordian corresponds to 20 m of distinctive brown chert limestones with a high silica content (Gottis *et al.*, 1967). This formation is missing here, potentially due to the extensional fault observed at 440 m.

From 550 to 630 m, the cores record a thick interval of black marls with calcarenites at the base, related to the late Middle Callovian. The calcarenites comprise polygenic intraclasts derived from a carbonate platform and bioclasts. The proportion of carbonates increases upwards, and the transition with the overlying Upper Callovian limestone is progressive.

From 630 to the bottom at 747 m, core samples alternate between dark grey marly wackestones and black marls, in several metres thick packages. While drilling, limestone intervals have revealed the presence of several artesian water flows. Drilling and coring stopped within a >50 m thick black marls sequence. Comparison with neighbouring outcrops and correlation with the regional lithostratigraphic column suggest a Middle Callovian age.

4.2 Deformation

The carbonates of the reservoir display distinct modes of deformation, according to the dominant lithology.

Limestones are affected by bedding-plane stylolites. They are more frequent in the marly mudstone intervals (Fig. 5a, and 5b). They are associated with thin (typically $\leq$1 mm) and short (typically several centimetre long) sub-vertical calcite veins, or centimetre-thick calcite-cemented pull-apart zones connecting several stylolites (Rispoli, 1981). Uncommon vertical stylolites, showing horizontal teeth are also observed in the limestone.

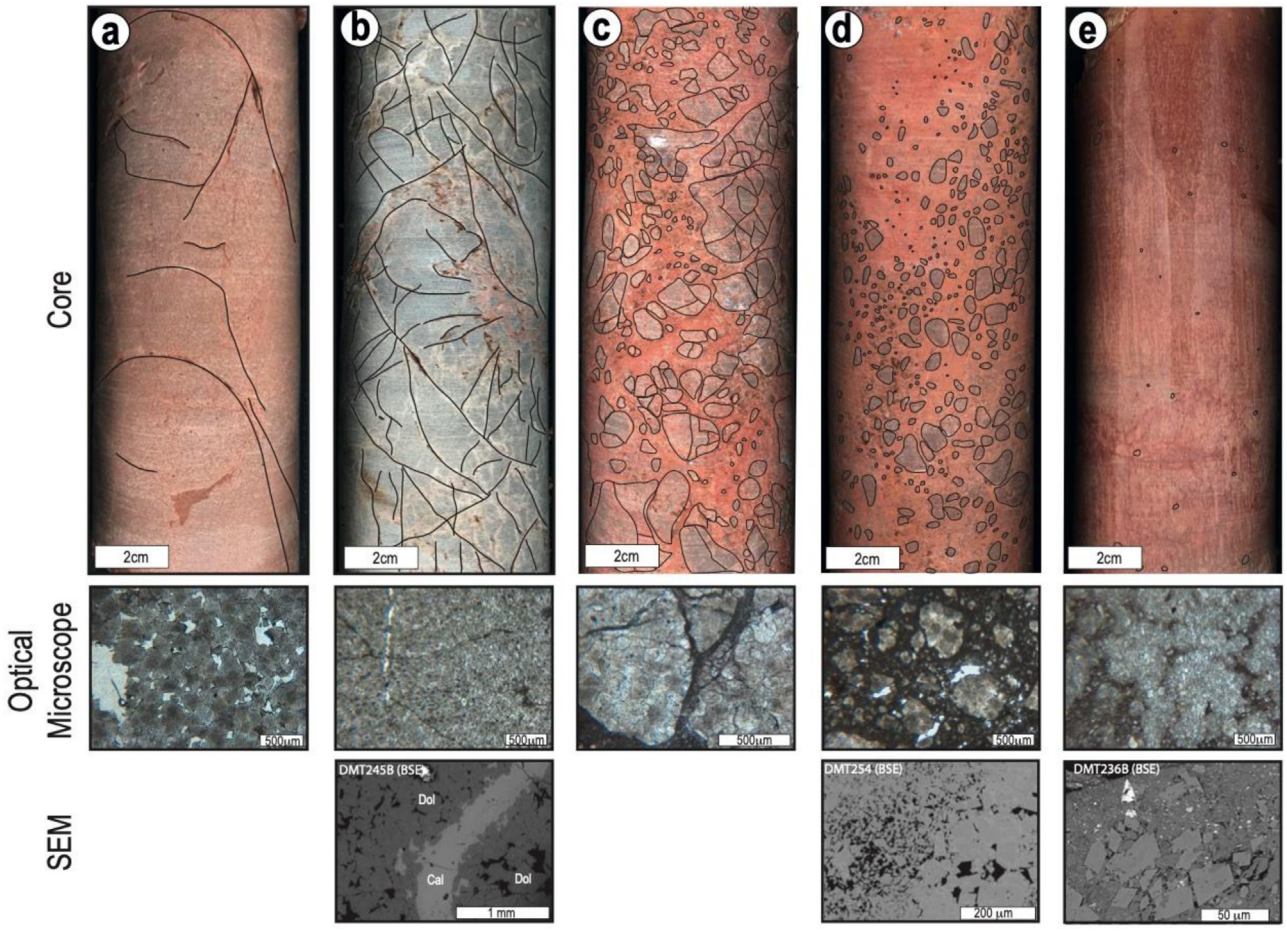

Fig. 6. Correlation of borehole optical imaging with the cores. This provides an orientation for the extensional fault planes and cataclastic faults zones observed in cores.

Brecciation in limestone results in sub-angular, centimetre-scale, clasts of limestone and white sparitic calcite, floating within a white calcite cement (Fig. 5c). Reddish silt and clay may also be present between the clasts. Such breccia contains stylolites that affect both clasts and calcite cement. These overall bedding-parallel stylolites, are sometimes rotated into oblique shear-zones (Hausegger *et al.*, 2010) (Fig. 5d). All observed features, *i.e.* stylolite teeth, orientation and rotation, or pull-apart zones infilled by calcite cement between oblique planes or stylolites, reveal a normal sense of shear displacement. Fault cores, typically several tens of centimetres wide, suggest a displacement of several tens of metres, according to the relationship between faultcores width and offset (Torabi and Berg, 2011). This type of deformation is particularly well expressed in the 157–210 m interval, in the footwall of the major fault, and, to a lesser extent, in the 440–550 m interval. In addition, such brecciation is observed locally along centimetre-scale fine shear-zones sub-parallel to bedding, in the 550–630 m interval (Middle Callovian) made of dark marly limestones and marls.

Another type of breccia is locally observed in limestones. It displays clasts with jigsaw geometry of the host-rock limestone and clasts of the earlier milky calcite veins, which are cemented by euhedral calcite. Such cement is observed penetrating into the host-rock, through multidirectional calcite small veins (Fig. 5e). Such features correspond to hydraulic brecciation of the limestone host-rock due to fluid pressure increase in veins or in the formation (Jébrak, 1997; Chauvet, 2019). Hydraulic fracturing is particularly well developed in the 450–500 m interval and also in several much thinner intervals ($\leq$1 m) between 540 m and 570 m.

Finally, all limestone intervals are affected by extension fractures filled with different types of calcite (see below). They are dominantly sub-vertical and often cogenetic withbedding-parallel stylolites. Other vertical or steeply-dipping planar fractures are open or not completely filled. Although mostly observed in limestones, some centimetre-wide open fractures affect the dolomite (*e.g.* at 300 m).

Dolomite is affected by pervasive brittle deformation, which overprints all initial sedimentary textures. The main dolomite interval (210–345 m) is entirely damaged, and it displays gradients of deformation, ranging from weak fracturing, through crushed breccia, to ultra-cataclasite (classification of Sibson, 1977, Figs. 3 and 6). Low-strain pervasive fractures (0.01–0.1 mm wide) are randomly oriented and form centimetre-scale spacing networks that individualise small ($\leq$1 cm) blocks of dolomite (Fig. 6a). Increasing amount of deformation results in dolomite micro-blocs individualization and rotation leading to a centimetre-scale puzzle-like texture (Fig. 6b). Next increase of deformation sees fracturing

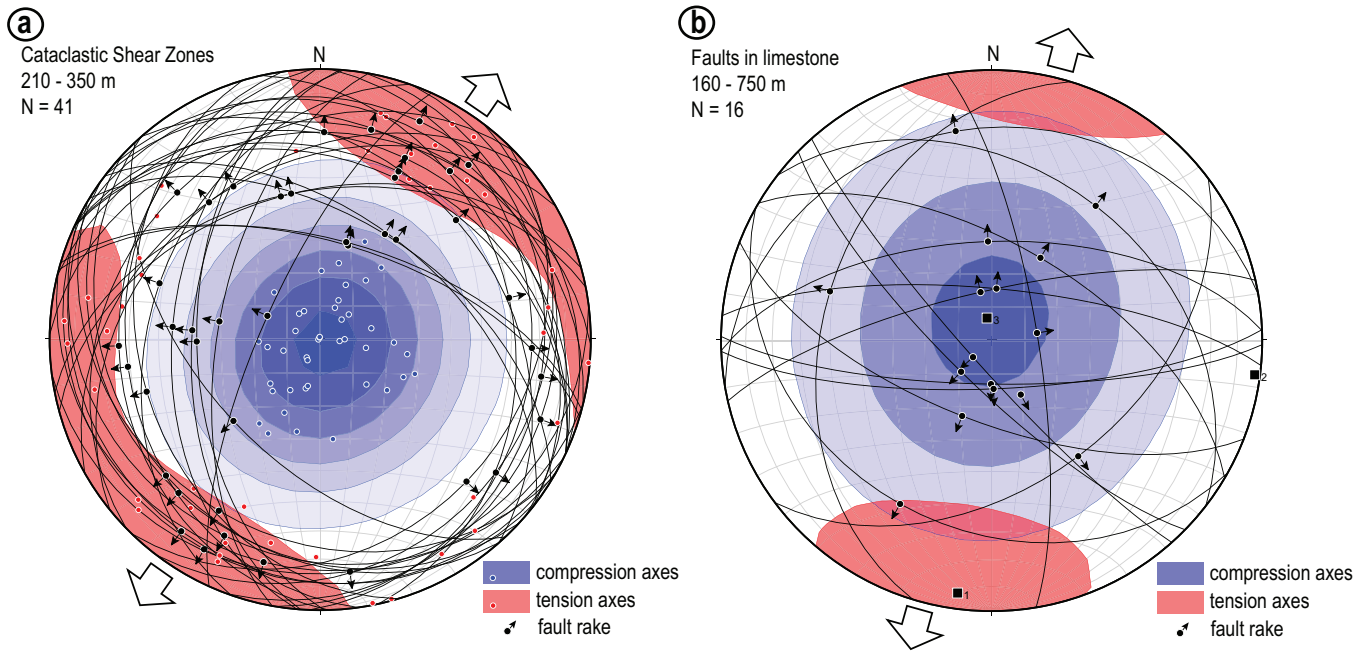

Fig. 7. a: Faultkin^{TM} representation of the cataclastic faults affecting the dolomites, that have been plotted on the borehole optical imaging and assuming a 90° rake (see text for justification of this assumption). It results in a NNE-SSW orientation of extension; b: similar process for normal faults in limestone; orientations, dips and an assumed constant 90° rake also provide a NNE–SSW direction of extension.

of the blocks accompanied by clasts translation and rotation (brecciation), within a matrix of reddish cataclased dolomite, representing up to 50% of the volume. In thin sections, fractures are seen filled with cataclastic dolomite material (Fig. 6c). Strain increase is expressed by increasing amount of fracturing and of cataclastic matrix (up to 75%), and clast size decrease (comminution, Fig. 6d). Maximum strain is expressed by cohesive, red, up to 10 cm wide, cataclastic to ultracataclastic shear zones, *i.e.* with no more than a few percent of host material preserved in the fault core. Thin-sections confirm the intense cataclasis of the dolomite, with clasts size lower than 1 μm in the matrix. These clasts show rhombohedral shape and clast-size distribution displays gradient consistent with micro-scale shear-bands, suggesting that comminution is achieved by fracturing along the dolomite crystal lattice.

4.3 Kinematics

Rotation of the clasts into the cataclastic fault zones suggests a normal sense of motion. However, their low angle of dip (<40°) is less than the classical 60° dip of andersonian normal faults. The cores that are affected by such cataclastic zones generally split along the plane of maximum strain localization, thus revealing slickenlines with high values of rake (>70°). .

From the borehole optical imaging, we picked and compiled both orientation and dip of 42 cataclastic fault zones affecting the dolomite reservoir. On the basis of core examination, we extrapolate that all cataclastic fault zones record a normal sense of displacement and a 90° rake. Such a hypothesis is not consistent with stress-tensor inversion methods (*e.g.* Célérier *et al.*, 2012), however, it allows us to determine the orientation of extension with the FaultKin8^{TM} software (Allmendinger *et al.*, 2012) (Fig. 7a). Stereonet shows quite dispersed cataclastic fault zones orientations, however, tension axes display a maximum around a NE–SW trend and a pression axis close to vertical, consistent with NE–SW extensional tectonic event.

Similar method including a similar hypothesis, applied to the brecciated faults observed in the limestone intervals, provides a similar direction of extension (Fig. 7b).

The faults observed in both limestones and dolomites, therefore correspond to a NNE–SSW oriented extension, expressed by distinct deformation modes depending on the lithology. These observations thus point to a penetrative deformation related to an extensional event that affected several metres-thick sections distributed throughout the whole reservoir (see log on Fig. 3a).

Only one normal fault of significant offset is observed on cores and on optical imaging of both parallel boreholes (#3 and #4) that are located 3 m apart. The fault borehole images provide orientations of 068° 30°N and 081° 60°N, respectively. The significant mismatch in fault orientation in the two boreholes suggests an uneven fault surface, with an average ENE–WSW orientation and 45° dip to the north. In association with the 90° pitch of the slickensides observed on cores, this orientation suggests a NW–SE extension (Séranne, 1999).

Extension fractures are observed on the cores. They are cemented with calcite and sometimes display polyphase filling. Extension fractures are also identified in the borehole optical imaging, although the details of cementation (color, crystal habits) cannot be distinguished. They were picked and compiled with the WELLCAD^{TM} software. Figure 8 represents the poles of 500 extension veins. The poles of veins are arranged in a girdle around the stereonet, which indicates

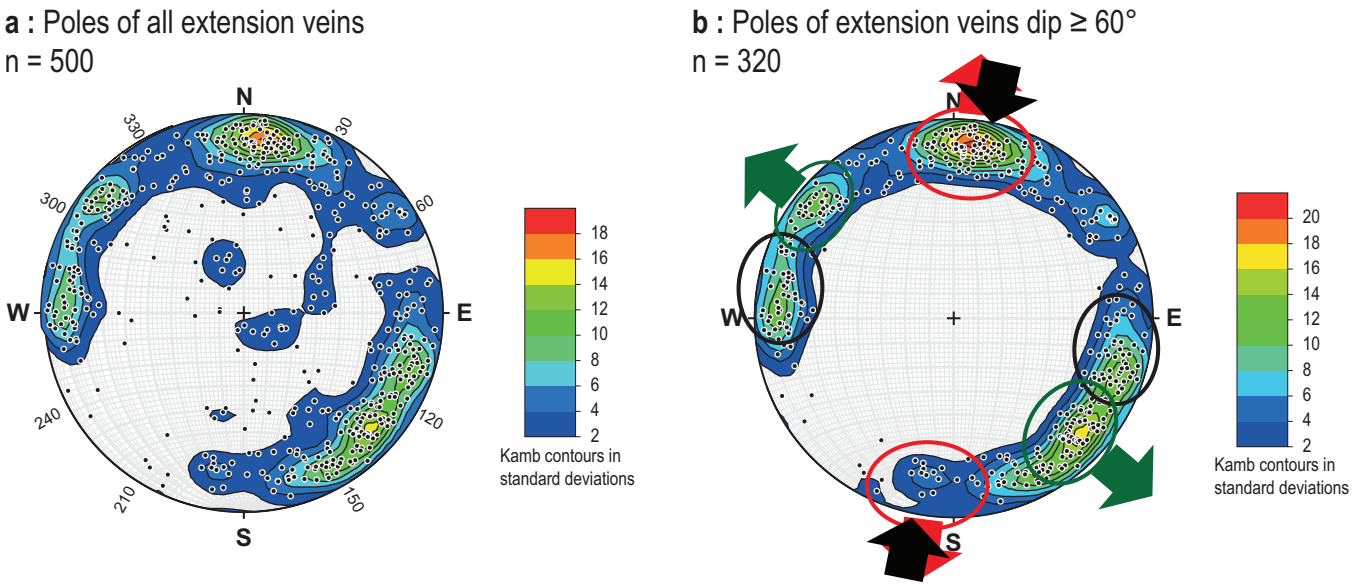

Fig. 8. a: poles of all extension veins measured on borehole optical imaging ($n = 500$), indicating mostly vertical to subvertical extension fractures, while the girdle distribution suggests superposed axes of deformation; b: analysis of the ≥60° dipping extension fractures ($n = 320$) indicates three distinct families, corresponding to NNE–SSW extension (red), NNE–SSW compression (black) and NW–SE extension (green).

high-angle to subvertical veins. There are also few poles in the central area of the stereonet, corresponding low-dip to sub-horizontal structures. Cross-examination and correlation with the cores reveal that structure with lower angle of dip corresponds to either bedding parallel shear-planes coated with calcite, or, to reactivated and crystallised fractures, specifically in the dolomite interval. In order to simplify the analyses and interpretations, we have selected the extension veins dipping 60 to 90°, which represent the overall dominant population ($n = 320$). Figure 8b shows 3 main groups of poles of subvertical extension veins that emerge from the girdle: 1: N–S poles, corresponding to E–W extension veins (red on Fig. 8b); 2: E–W poles, corresponding to N–S extension veins (black on Fig. 8b); and 3: SE–NW poles (green on Fig. 8b).

The E–W oriented extension veins are consistent with a N010°–N0190° extension; we therefore relate them with the extension of the same direction responsible for the formation of the normal faults. Observation on cores shows that the subvertical N–S extension veins overprint the faults zones, both brecciated fault cores in limestones and cataclastic faults cores in dolomites. No cross-cutting relationships could be observed with the major normal fault, however, the latter is consistent with the third cluster of tension gashes corresponding to NW–SE extension, and we suggest that they belong to the same extensional event.

5 Alteration of the carbonate reservoir

5.1 Karstification

The cores reveal three distinct types of karst, according to their filling and to their position within the reservoir.

The top of the Jurassic carbonates reservoir is karstified, with dissolution structures and extending 15 m downward (from −75 to −90 m). In addition to the metre-scale karst cavities that were detected during drilling operations (see above), the cores show evidence of Lapiaz, or karst cavities of several centimetres wide, are filled with the overlying marine sandy marls of Burdigalian age (Fig. 9a). Karstification was achieved in subaerial conditions, prior to the transgression, of which the marine sediments unconformably overlie and seal the palaeo-epikarst.

Deeper karst structures extend in the limestones of the upper reservoir (−120 to −210 m, Fig. 9b). Centimetre-wide dissolution cavities affect both deformed (faulted and brecciated) and pristine carbonate, as well as calcite veins. Such karsts are presently hydrologically active, as shown by water flows during drilling (*e.g.* around 137 m). Others karsts are plugged by polyphase filling, including pink laminated silts, Burdigalian marls and calcite cements.

The major dolomite reservoir (210–347 m) does not show evidence of karstification, although dolomite outcrops observed in the close surroundings of the borehole display metre-scale structures interpreted as resulting from dissolution.

Very deep karst structures are found in the −450 to −500 m limestone interval. This endokarst is characterised by ≤10 cm wide dissolution cavities, which are superimposed onto fractures partially filled with white coarse calcite spars (Fig. 9c). Cavities are clogged by bright red silty clays, which may contain fine clasts of oxi-hydroxydes derived from laterite crust. These observations indicate that (i) meteoric fluid-driven dissolution was guided by a previously acquired fracturation; (ii) the base level was lower than the observed interval, whether this resulted from sea-level drop and/or the carbonate massif was then at higher elevation; (iii) the karst network was affected by high-energy hydrodynamics able to carry surface sediments 500 m downward, into the fractured and karstified massif. Oxidising conditions also support a water-table level lower than the observed karst fill (Travé *et al.*, 2021).

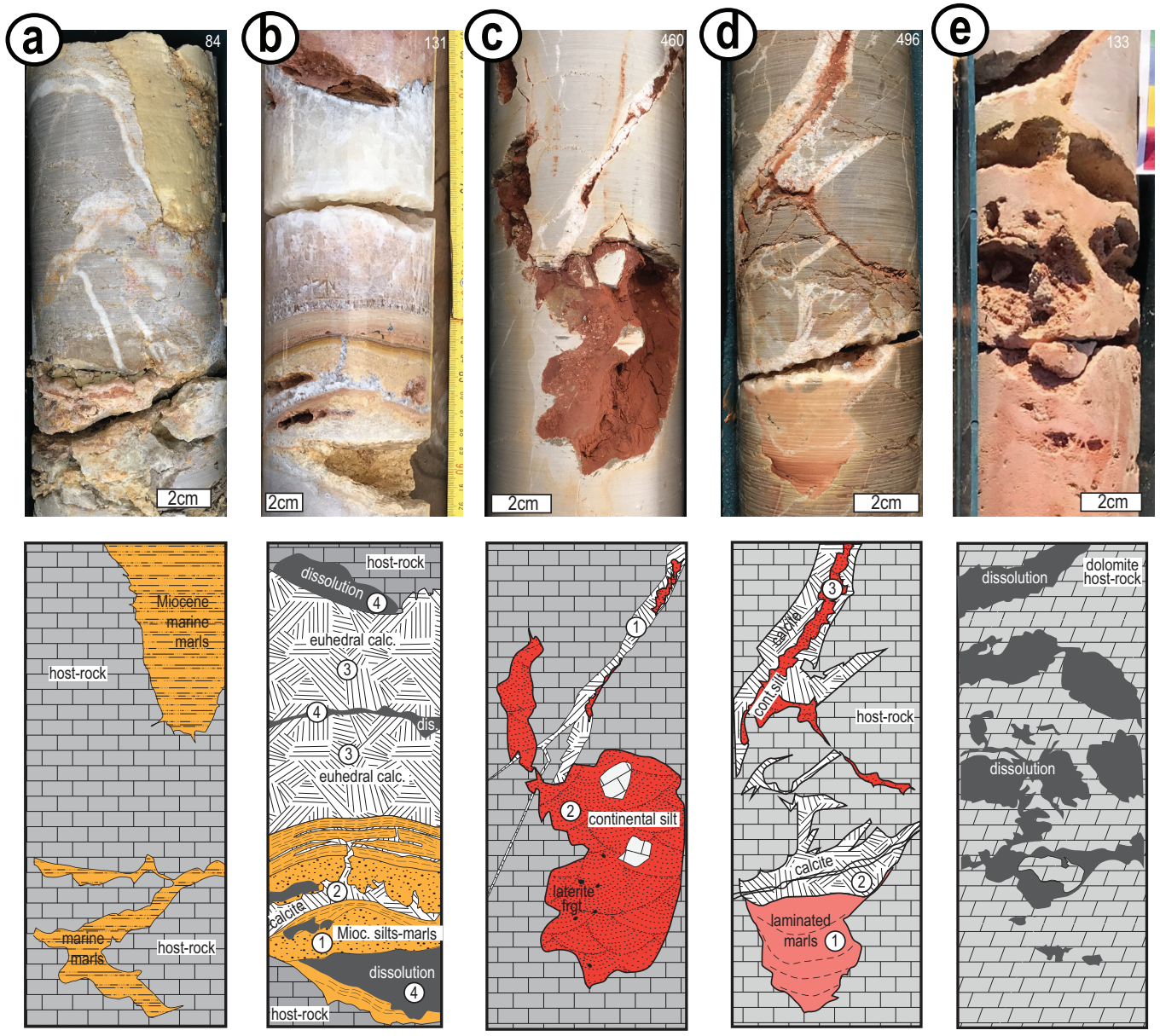

Fig. 9. Different types of karsts observed in cores (top panels, white number indicates the sample depth) and interpreted (lower panels): a: palaeo-epi-karst at the top of the Jurassic reservoir; it is sealed by marine Miocene sediments; b: complex paleo-endokarst partly filled with laminated silty marls of Miocene age, and with euhedral calcite cement; the host-rock, karst fill and cement were later affected by dissolution; c: karstification of both host-rock and cracks mineralized with calcite: both are filled with continental lateritic red silty clay transported down to 460 m deep in the reservoir by active hydrodynamics; d: karstification of limestone partly filled by laminated lithified ochre and pink marls (1), followed by calcite cement (2) and lateritic silt (3); e: dissolution in dolomite, such connected cavities are obsereved where water flux was documented during drilling.

Another type of karst infill is observed in that 450 to 500 m deep interval, in the upper Callovian formation. The lack of emersion structures (desiccation, brecciation, transgressive lag) in this marine interval indicates that such karsts are not early, syn-depositional features. The karst filling consists of lithified laminated marl, of ochre to pink color, and which are older than the red continental sits karsts-infill (Fig. 9c).

Finally, the carbonates of the upper reservoir displays connected, centimetre-scale cavities (Fig. 9e). Where dolomitized, the host-rock shows high porosity textures, whereas limestones of that interval shows cavities with corroded walls and no infill nor cement. While drilling, such intense dissolution intervals revealed water influx; the larger one was recorded at 132–134 m depth (Figs. 3 and 9e).

5.2 Dolomitization and calcitization

The cores reveal dolomitization affected two types of limestones. Firstly, the oolite grainstone of Tithonian age from the upper reservoir (Fig. 10a) shows multiple, complex and

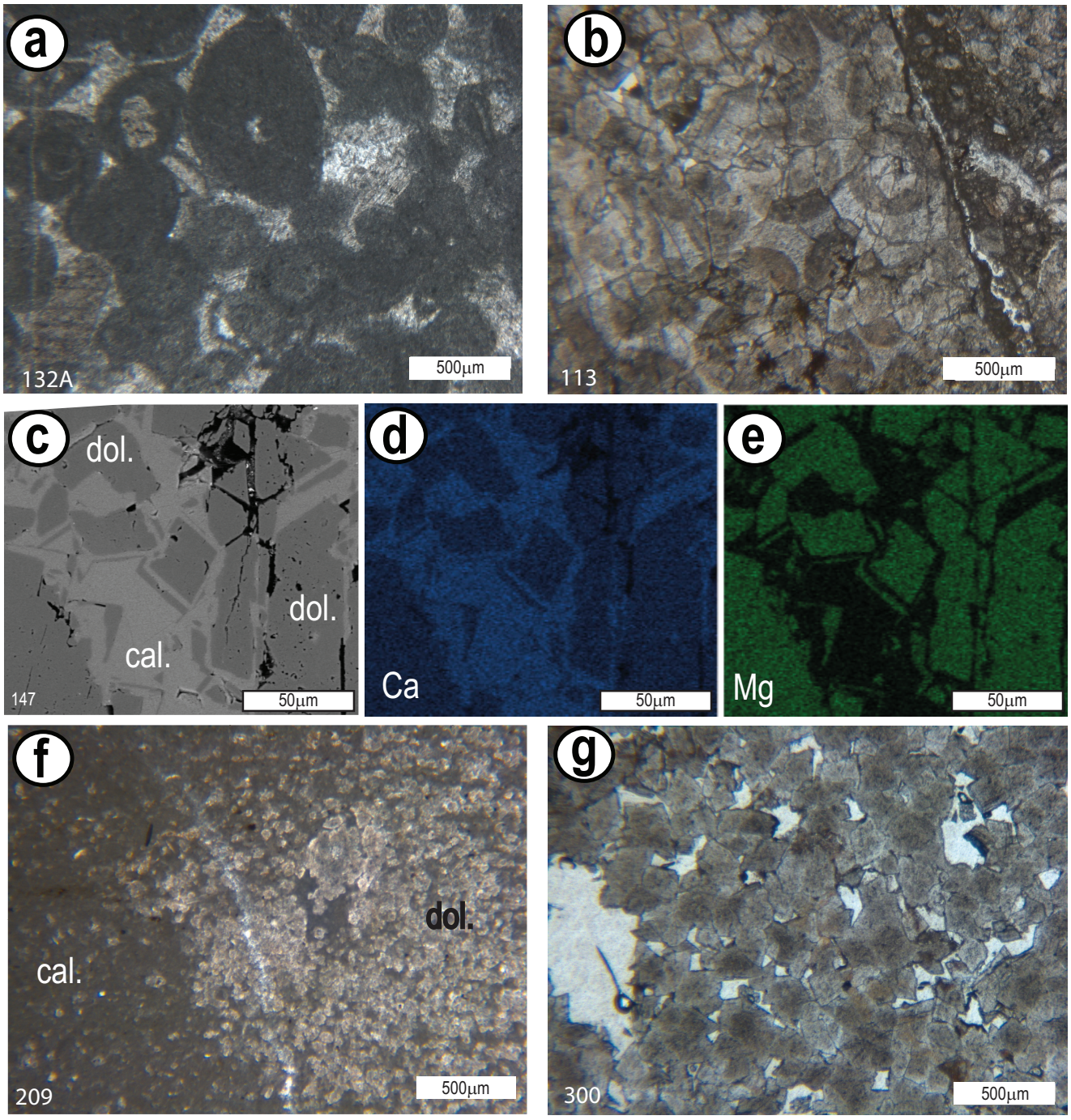

Fig. 10. a: original oolitic grainstone of the upper reservoir (plane-polarized light); b: dolomitized grainstone showing oolithe ghosts; it is affected by cataclase observed on the right (cross-polarised light). The upper reservoir provides evidence of dissolution of calcite and successive dolomitization and dedolomitization, as shown by SEM image (c). SEM chemical mapping of Ca (blue, d) and Mg (green, e) displays successive zones of calcite and dolomite, respectively; f: dolomitization front of the mudstone in the lower reservoir (natural light; cal.: calcite; dol.: dolomite); g: dolomite in the lower reservoir showing a significant amount of porosity (plane-polarized polarised light).

irregular dolomitization fronts (74 to 157 m). Such dolomitized intervals are found within the interval containing 0.1 to 1 m-wide karst conduits that are associated with present-day water circulation, as detected during drilling. Thin-sections show the original oolitic porous texture preserved as ghosts within a texture of large crystals of dolomite (Fig. 10b). Calcite replacement by unimodal, small, planar euhedral crystals of dolomite, in several interdigitated zones within the shallowest part of the reservoir may suggests dolomitization driven by marine water-flow through the highly porous limestone (Vahrenkamp and Swart, 1994), but other kinds of dolomitizing fluids cannot be ruled out. Dedolomitization or dolomite

calcitization (Coniglio, 2003; Radwan *et al.*, 2021) is demonstrated by corrosion of dolomite crystals, subsequently coated by calcite growth and internal calcite zones within rhombs. Other rhomboedric crystals display alternate fringes of Ca and Mg distribution in SEM imaging, suggesting alternating calcite and dolomite (Fig. 10c–e). Such microscopic evidence of successive dolomitization/dedolomitization is observed across the whole interval of the upper reservoir (75–157 m), although it is more frequent in the top of the Jurassic reservoir, between 75 and 90 m. This oolitic upper reservoir is therefore highly porous and affected by a network of karst conduits, with evidence of past and present circulations of both dolomitizing fluid and freshwater (karstification).

Secondly, the lower reservoir between 210 and 335 m depth features a complete dolomitization of mudstone and clayey limestone of Lower Kimmeridgian and Upper Oxfordian age. Dolomite texture appears as unimodal, planar, euhedral small (10 to 50 μm) rhombs, in a matrix consisting of the initial micritic limestone (Fig. 10f). Dolomitization resulted in a compact, saccaroid rock, which is intensely fractured. Fractures are presently filled with fine crystallined calcite. No evidence of dedolomitization processes was observed in this lower reservoir. Drilling operations recorded evidence of present-day water circulation in one major, 5 cm-wide, sub-vertical crack, at 298 m depth. This crack displays calcite crystallisation along the walls and remains open in the centre. The homogeneous dolomitization of the mudstone is constrained upward by clayey centimetre-thick interbeds that may have acted as seals. This suggests that dolomitization of the 130 m-thick interval, beneath a >150 m-thick cover, could result from a deep-seated process, linked to an ascending fluid flow

6 Signature of different fluids

The mineralizations observed in veins and fractures are signatures of the different fluid flows within the carbonate reservoir. Analyses of the distribution of these mineralizations, as well as their geometric, macroscopic and microscopic features, observed under natural and cathodoluminescence light, provide clues about the relative chronology, the nature and origin of the fluids (*e.g.* Labaume *et al.*, 2004; Travé *et al.*, 2007; Laurent, 2015). Five types of crystallisation have been distinguished in the cores:

- calcite crystallised in the sub-vertical fractures associated with bedding-parallel stylolites presents the same red-orange luminescence as the surrounding mudstone (Fig. 11a). This supports a closed hydrological system with short distance transfer by diffusion of calcite dissolved in the stylolites to the neighbouring fractures where it precipitated (Gratier *et al.*, 1999; Toussaint *et al.*, 2018);
- white scalenohedral calcite is observed filling geodes and centimetre-wide veins in the lower dolomitic reservoir (Fig. 12). Geodes usually appear at the top of brecciated zones. Dolomite puzzle-shaped clasts float in the calcite that fills the veins and secondary, smaller-scale calcite veins penetrate the host dolomite (Fig. 12c). This suggests hydraulic fracturing; (*e.g.* Jébrak, 1997). Scalenohedral calcite appears in cathodoluminescence with a dark-red color (Fig. 11b). The absence of varying luminescence zones indicates a constant chemistry of the mineralizing fluid throughout crystallisation, and/or a fast crystallisation process;
- orange calcite crystals are observed cementing the breccia developed in the damage zone of normal faults related to the NNE–SSW extension. In these intervals, orange calcite is also observed sealing the normal faults planes and filling the re-open sub-horizontal stylolites. It is also found coating the walls of one major crack (298 m). In plane polarized light, the orange calcite appears to incorporate significant concentrations of iron oxi-hydroxides (Fig. 11c). In CL, this calcite appears as mottled, with weakly luminescent areas. In rare occurrences, orange calcite can also be observed as a secondary cement, overprinting translucent calcite (see below), in centimetre-wide sub-vertical veins;
- translucent white calcite is observed filling up sub-vertical fractures and matrix porosity (Fig. 11d). In addition, this calcite often crystallises within dissolution structures, such as corrosion pits in the host limestone or in earlier calcite crystals. In plane polarized light, this calcite appears as large crystals filling completely the vein, whereas it is totally opaque in CL (Fig. 11d). Such black CL may indicate a precipitation of fresh-water (Labaume *et al.*, 2004; Bussolotto *et al.*, 2015), but additional geochemical analyses are needed to confirm this. Translucent calcite is found throughout the whole borehole, although it is prevalent in the upper reservoir (75–165 m);
- euhedral dogtooth calcite crystallised in subvertical, open, centimetre-wide cracks, presents successive growth generations, characterised by varying colors (white, light orange) sometimes separated by dark films. In natural light, this calcite appears as large clear crystals and the dark films correspond to patches of iron oxi-hydroxydes (Fig. 11e). In CL, the large crystals show a succession of thin zones that range from very luminescent to opaque, through dark red. The drastically different CL of successive calcite growth zones in the sub-vertical veins characterises temporal variation of fluid composition, and/or varying redox conditions in groundwaters at the time of growth (Meyers, 1991; Milodowski *et al.*, 2018).

The cross-cutting relationships of the mineralized veins and fractures allows to establish a relative chronology of events and associated fluid-flows (Fig. 13).

7 Discussion

7.1 Chronology of events

The observed structural relationships indicate a relative chronology of tectonic events while structural analyses allow to determine directions of extension and shortening, which can be correlated with regional geodynamics, in order to construct a calendar for the evolution of the reservoir (Fig. 14).

Following Late Jurassic carbonate deposition and early diagenesis (not addressed here), bed-parallel, compaction-related, stylolites and related calcite-cemented veins are the earliest observed structures.

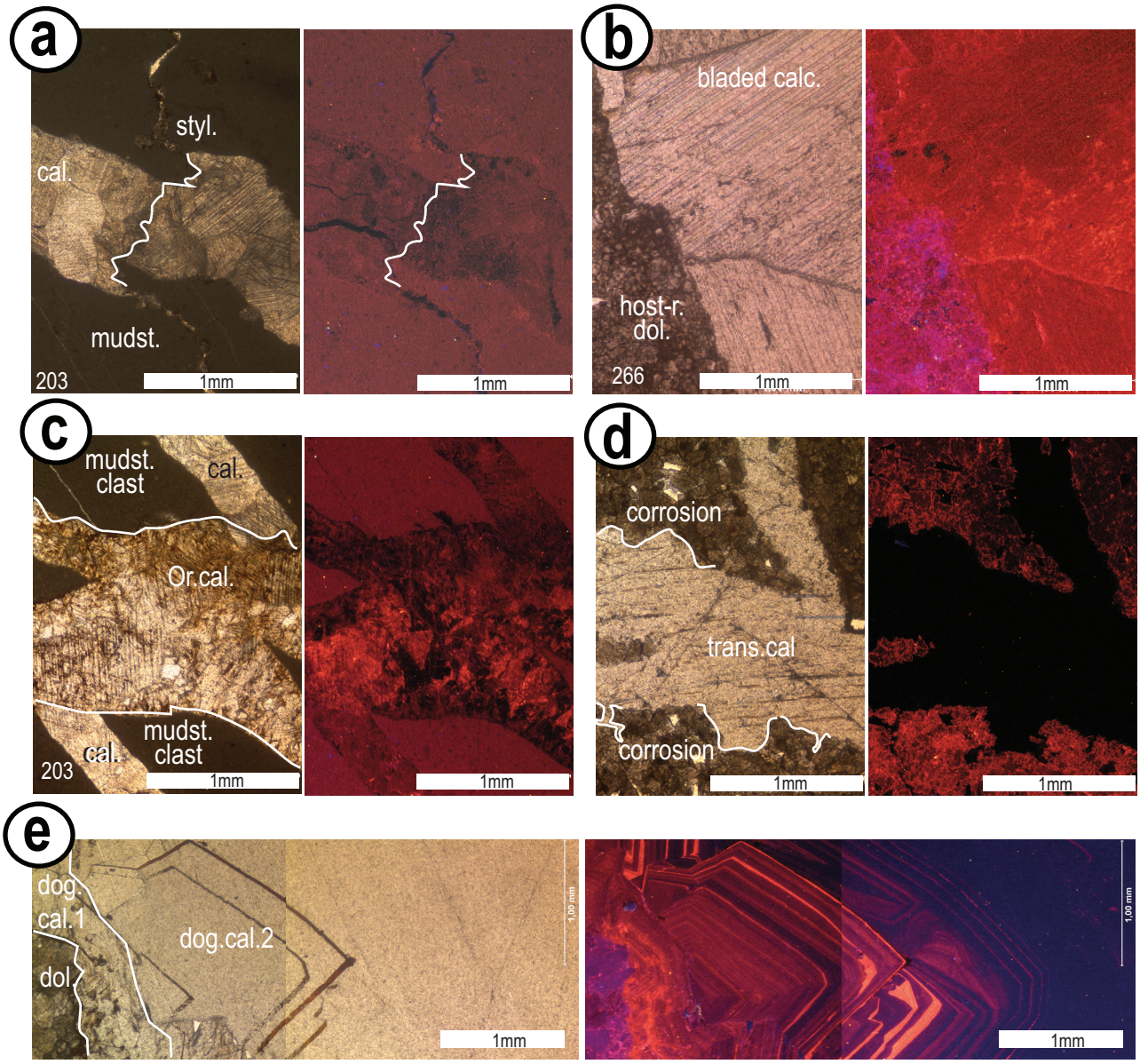

Fig. 11. Microphotographs of the 5 different types of calcite mineralizations, each sample is illustrated by a view in natural light (left) and in cathodoluminescence (CL, right): a: sub-vertical calcite vein associated with compaction-related stylolites (white line); b: scalenohedral calcite in dolomite host-rock; in CL, bright orange bladed calcite contrasts with purple-pink dolomite host-rock; c: orange calcite in natural light (Or. cal.) in fault breccia comprising mudstone clasts, some of them including earlier calcite veins (cal.) and dark oxi-hydroxides elements; in CL, this calcite appears as non-homogeneous bright red areas including smaller darker or black zones; d: translucent calcite (trans.cal.) filling corrosion structures; e: dogtooth calcite (dog.cal.), the CL color bands indicate varying chemistry of the fluid, including bright orange (thermal), dark red and black (meteoric origin). CL photographs have been lightened by 10 to 30% to improve visibility but colors have not been modified.

The whole reservoir, including compaction-related stylolites is affected by normal faults in limestones and cataclastic shear-bands in dolomites. Borehole Optical Imaging has allowed to orientate such structures corresponding to a NNE–SSW extension (Fig. 7), which represents the major and most distributed deformation across the reservoir. These extensional structures are consistent with the WNW–ESE-oriented extension veins and fractures (Fig. 8) and we interpret them as resulting from the same tectonic setting. Crystallization of the orange calcite cements the brecciated fault cores and clearly overprints bedding-parallel stylolites and associated calcite veins. We interpret the orange calcite cement as contemporaneous with these normal faults

Such NNE–SSW direction of extension is not documented in the study area (Arthaud and Laurent, 1995). However, there are tectono-stratigraphic evidences of syn-bauxite deposition block-faulting in Languedoc (Hemelsdaël *et al.*, 2021b). In addition, similar direction of extension has recently been recorded in the nearby Late Jurassic limestones that are karstified and filled by bauxite, dated to the Albian (Marchand,

2019; Marchand *et al.*, 2020). Furthermore, direct U-Pb dating of calcite on slickensides of strike-slip and normal faults consistent with NE–SW extension, in several localities of Languedoc yield Aptian to Cenomanian ages (Parizot, 2021). We therefore relate the NNE–SSW extension to the late Early-Cretaceous pre-orogenic rifting of the Pyrenees and offshore Provence (*e.g.* Tavani *et al.*, 2018 and references herein), simultaneously to the uplift of the south-European margin, locally known as the "Durancian Uplift" (*e.g.* Marchand *et al.*, 2020 and references herein). In Languedoc, this uplift induced denudation of the Early Cretaceous carbonate cover by combined erosion and karstification, down to Malm sequences (Chanvry *et al.*, 2020; Marchand *et al.*, 2020). However, the studied cores do not provide evidence of karstification related to Durancian; in particular, the distinctive marker of this event – bauxite – has never been observed in the small karstic cavities of the cores. This is consistent with the palaeogeography derived from analyses of the neighbouring outcrops, where karsts filled with bauxite do not extend more than several metres below the bauxite deposits, which feature the palea-baselevel (Marchand, 2019). Cretaceous karstification has affected only the sedimentary interval above the Jurassic sequence sampled by the cores.

Extensional shear-bands and faults affect the dolomite of both the lower and upper reservoir. Furthermore, cataclasis and comminution of the dolomite material documented in the lower reservoir (Fig. 5d) indicates that dolomitization predates or is contemporaneous with the extensional tectonics corresponding to the "Durancian Uplift". Dolomite intervals in the upper reservoir display similar structural relationship and deformational evidences of a pre-tectonic dolomitization event. However, dolomite in the upper reservoir also reveals evidence of successive calcitization and dolomitization phases that are markedly absent in the lower dolomite reservoir.

The setting of the lower dolomite reservoir, covered by a marly limestone acting as a cover suggest deep dolomitization by an ascending fluid. This may correspond to a burial dolomite model, where basinal brines migrate from the deep and subsiding basin (Stacey *et al.*, 2020), assisted by faults (Davies and Smith, 2006; Benjakul *et al.*, 2020). The location of the study area on the western margin of the Tethys during Jurassic may account for the rise of thermal fluids (in the sense of (Machel and Lonnee, 2002) from the highly subsiding eastern part of the basin, during Jurassic times (Debrand-Passard and Courbouleix, 1984). Alternatively, dolomitization of the lower dolomite reservoir may be related to ascending basinal fluids related to the renewed subsidence that occurred south of the study area, during Valanginian-Barremian times (Séranne *et al.*, 2002; Tavani *et al.*, 2018; Marchand *et al.*, 2020), prior to the extensional tectonics of the "Durancian Uplift". There is no unequivocal evidence that the pre-tectonic, first stage of dolomitization affecting the upper reservoir was contemporaneous. Timing of the additional calcitization/dolomitization events overprinting the upper reservoir is poorly controlled.

The subvertical N–S-oriented veins that affect the whole reservoir (Fig. 8) are tentatively interpreted as a result of NS compression. The unoriented cores display some vertical stylolites and rare reverse micro-faults (unfortunately, not visible on borehole imaging, thus not oriented) that confirm the existence of a compressive episode. Such compressional structures are overprinted onto the Cretaceous extensional structures, as observed in the outcrops (Marchand, 2019; Hemelsdaël *et al.*, 2021b). We correlate this deformation with the Pyrenean orogeny, which is the only shortening event that affected the Mesozoic carbonate platform of Languedoc, between the Maastrichtian and the Eocene (Arthaud and Laurent, 1995; Arthaud and Séguret, 1981; Hemelsdaël *et al.*, 2021b). Folding and thrusting may have been accompanied by karstification of the uplifted and exposed Jurassic limestones. In the 450–500 m interval, cores show karstic cavities with laminated mudstones, later covered by laterite-related silts (Fig. 9d). The age of such deep karsts is questionable. Lack of Miocene-age tracers in the infill, such as the marine yellow marls observed in the shallower karsts, argues for a karstification phase older than Messinian. The laterite-derived infill corresponds to Late Cretaceous to Paleocene residual covers found in the area (Bruxelles, 2001; Séranne *et al.*, 2002). The 500 m vertical amplitude of karstification suggests a combination of massif uplift and base level-drop, which could be correlated with the Maastrichtian-Early Paleocene initial phase of the Pyrenean shortening (Arthaud and Laurent, 1995; Hemelsdaël *et al.*, 2021b) and the repeated base-level drops that have been documented during the Danian and the Selandian in the area (Combes *et al.*, 2007; Husson *et al.*, 2012; Husson, 2013).

Another episode of extensional tectonics is marked by a single major normal fault at 157 m depth, that offsets all previous tectonic structures. Its NE-strike and its relative chronology are consistent with the Oligocene-Early Miocene NW–SE rifting of the Gulf of Lion (Séranne, 1999; Hemelsdaël *et al.*, 2021b).

Identification of Miocene marls in the karstified limestone as deep as 210 m provides clues for its evolution: karstification implies a base level drop of ≥210 m, associated with hydrodynamics able to transport downwards sediments deposited on the surface, and which postdates the Miocene. This is consistent with the Messinian base-level drop, which is known to have generated deep karst in the emerged carbonate platform of the area (Audra *et al.*, 2004; Husson *et al.*, 2018).

Finally, dissolution cavities in the upper reservoir overprints the Messinian-related karst (Fig. 9b). They are interpreted as the most recent karstification and the presently active water flows recorded during drilling, may suggest that the karstification process is still active.

7.2 Long-term evolution versus present-day water circulation

The structure of the carbonate reservoir therefore results from a long-term evolution, and the crystallisations attest of fluid circulations that have occurred from the Jurassic deposition and compaction to present-day. Interactions and/or successive flows of marine, meteoric and ascending waters seem to have controlled the post-depositional long-term evolution of the reservoir; yet present-day fluid interactions involve the same type of waters. It is unlikely that the paleo-fluid circulations remained similar throughout the long-term evolution, until today. Indeed, the present-day fluid interactions are controlled by the large-scale structures of the reservoir, which have been acquired during successive stages.

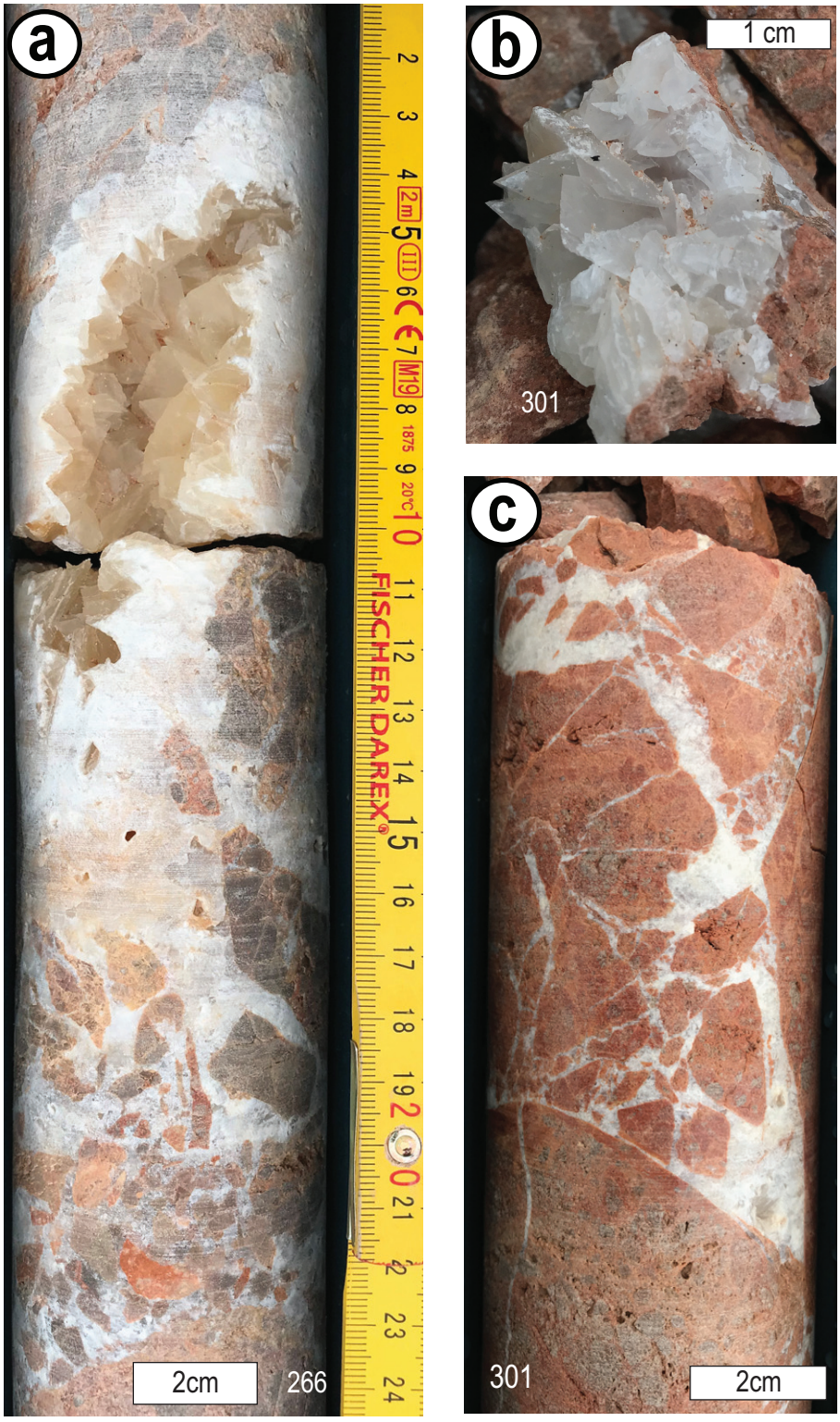

Fig. 12. a: core photographs of white scalenohedral calcite crystallised in a geode connected to veins formed by hydraulic brecciation of the dolomite host-rock; b: detail view of the bladed habitus; c: hydraulic breccia cemented by white bladed calcite.

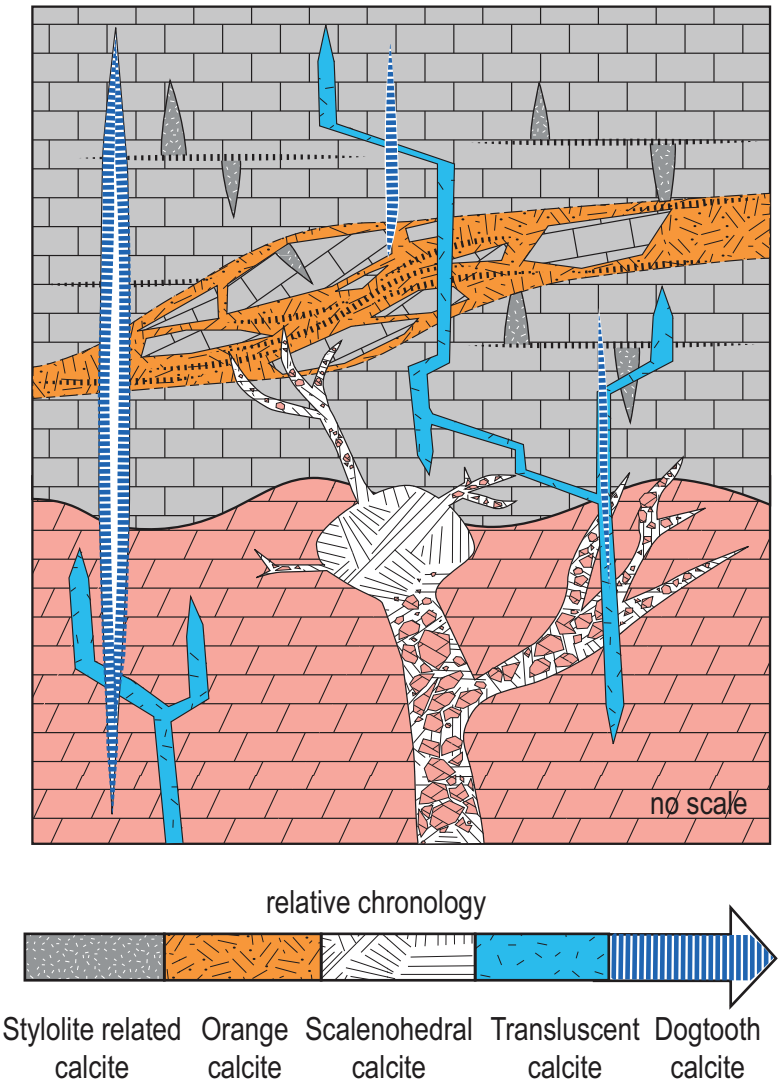

Fig. 13. Cross-cutting relationships of the different types of veins and calcite fills. The sketch (no scale intended) illustrates the relative chronology of the fluids from which the different calcites precipitated. The dolomite front represents the top of the lower dolomite reservoir (210–320 m).

Specifically, present-day thermal waters are drained upward by the Thau Thrust, a Pyrenean (Eocene) structure (Pétré *et al.*, 2020; Ranchoux *et al.*, 2022; Ladouche *et al.*, 2022); the thermal waters are sourced in a deeply buried limestone Jurassic reservoir (Ranchoux *et al.*, 2022; Ladouche *et al.*, 2022) that 3D geological modeling locates in the hanging-wall of the Nîmes fault, beneath more than 2 km of syn- and post-rift sequences, as a result of the Oligocene-Aquitanian rifting of the Gulf of Lion (Fig. 2) (Hemelsdaël *et al.*, 2021b). Furthermore, the hydrosystem that produces the thermal waters at Balaruc-les-Bains cannot predate the youngest structural element of the reservoir, *i.e.* deposition of the Pliocene cover.

7.3 Dolomitization/dedolomitization

Our observations suggest that a first stage of dolomitization of the Malm limestone occurred during Early Cretaceous, probably in relation with the Durancian uplift. In the upper reservoir (75–157 m), preservation of texture in the oolitic carbonate suggests low-temperature dolomitization at shallow level, seawater being the source of Mg (Machel, 2004). In addition, the alternate dolomitization/dedolomitization processes observed only in this upper reservoir indicates superimposition of an alternation of meteoric, freshwater and marine water circulations. It could be hypothesised that it is related to the temporary flux reversals of the submarine Vise spring (Pétré *et al.*, 2020). During normal (*i.e.* most frequent) setting, meteoric water is circulating in the upper reservoir, the carbonate host-rocks are karstified by CO_2-rich waters, and freshwater is outpouring at the bottom of the laguna (Fig. 15). During reversal of the spring ("inversac"), brackish to marine water penetrates the reservoir through the Vise spring, and extends across a kilometre-wide area (Pétré *et al.*, 2020). However, such reversals of the sub-marine spring are too short-term to account for the dolomitization of the underlying carbonates, leached by the salty waters at temperatures less

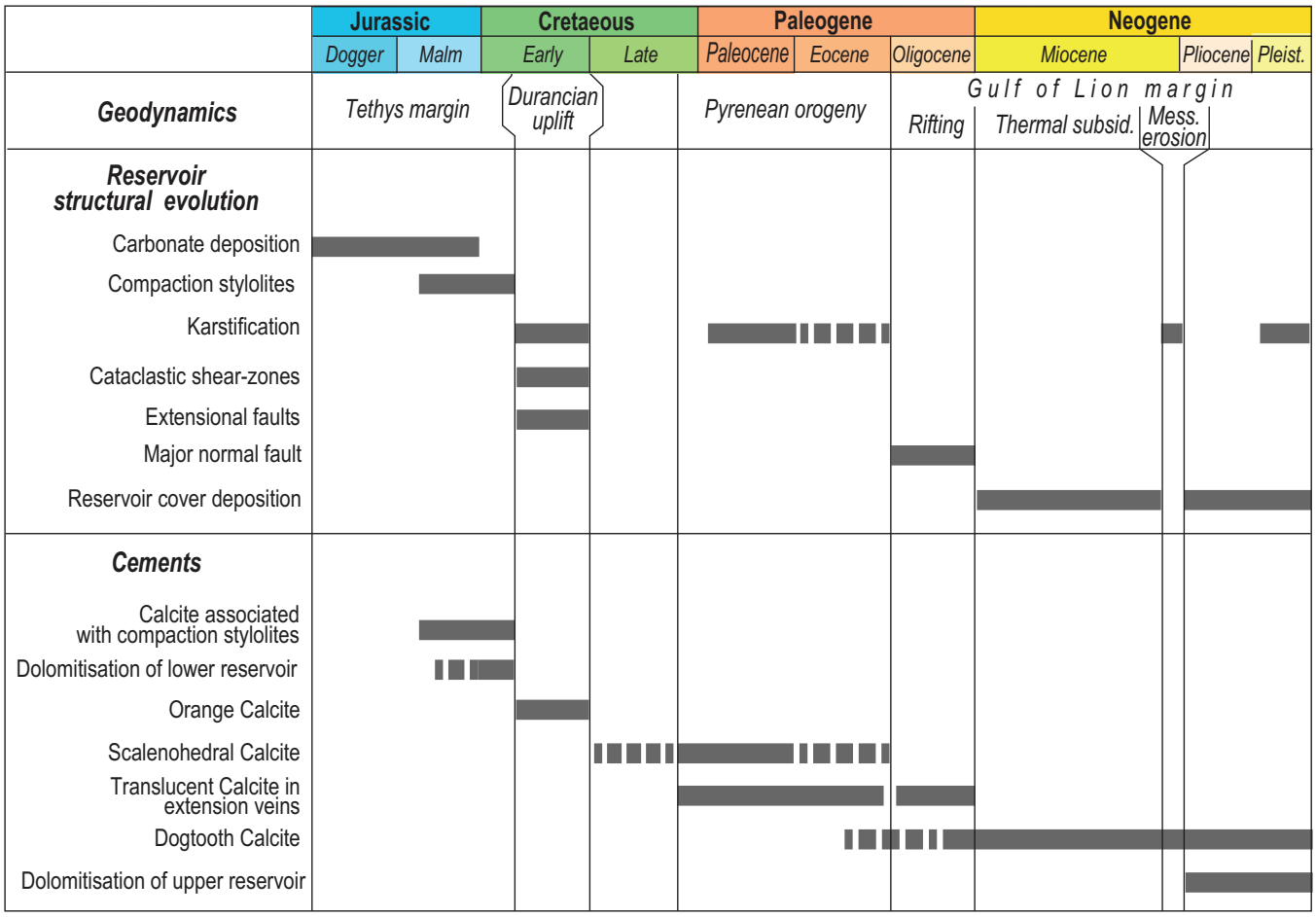

Fig. 14. Simplified chronological chart of the succession of events that affected and shaped the carbonate reservoir, in response to the geodynamic evolution of the region. The lower panel tentatively correlates the successive cements with the geodynamic evolution.

than 25 °C (Kaczmarek and Thornton, 2017) (Fig. 15). Alternatively, longer period oscillations, such as the Pleistocene glacio-eustasy sea-level changes, could be the driving mechanism for the oscillatory dolomitization and calcitization, as described by (Soreghan *et al.*, 2000). During interglacial high-stand, as today, seal-level reaches the carbonate massifs outlining the coastline; temporal imbalance between karstic fresh water level and marine water pressure results in marine-water invasion of the reservoir and dolomitization. During glacial low-stands, which record up to 100 m sea-level drops, the shoreline regresses up to 70 km basinward (Rabineau *et al.*, 2005). Consequently, the area of investigation is exclusively submitted to meteoric water, which reactivates karstification of the carbonates and allows calcitization, in the upper reservoir.

Alternatively, the dolomitization-calcitization episodes affecting the upper reservoir may correlate with longer period events. Specifically, transgressions allow seawater to penetrate carbonates that were previously exposed and karstified (Machel, 2004; Moss and Tucker, 1996). The present-day large-scale structure of the study area was acquired after the Gulf of Lion rifting, in Oligocene-Aquitanian times. Since that time, marine transgressions have covered several times the exposed and previously karstified Jurassic limestones of the study area (Husson, 2013). During the Burdigalian post-rift transgression, sea-level rise was recorded by onlapping shore sediments as high as 80 m elevation, on the hills surrounding the study area (Combes *et al.*, 2007). Later, following the Messinian desiccation event and deep karst formation, re-flooding of the Mediterranean allowed deposition of littoral Pliocene sediments some 10 m higher than the present-day sea-level (Gottis *et al.*, 1967). Therefore, the carbonates massifs of the study area and the Vise spring have been covered by marine water, which allowed salty water intake and interaction with the upper carbonate reservoir, leading to dolomitization (Fig. 15). Conversely, Messinian desiccation of the Mediterranean and glacial periods of the Pleistocene witnessed continentalization of the area, with formation or reactivation of karsts by circulation of meteoric waters and karstification of the exposed Jurassic limestone (Lofi *et al.*, 2012).

8 Conclusion

The karst reservoir of Thau-Balaruc, located across the shoreline of the Gulf of Lion passive margin, concentrates three distinct water fluxes (karstic freshwater, marine water,

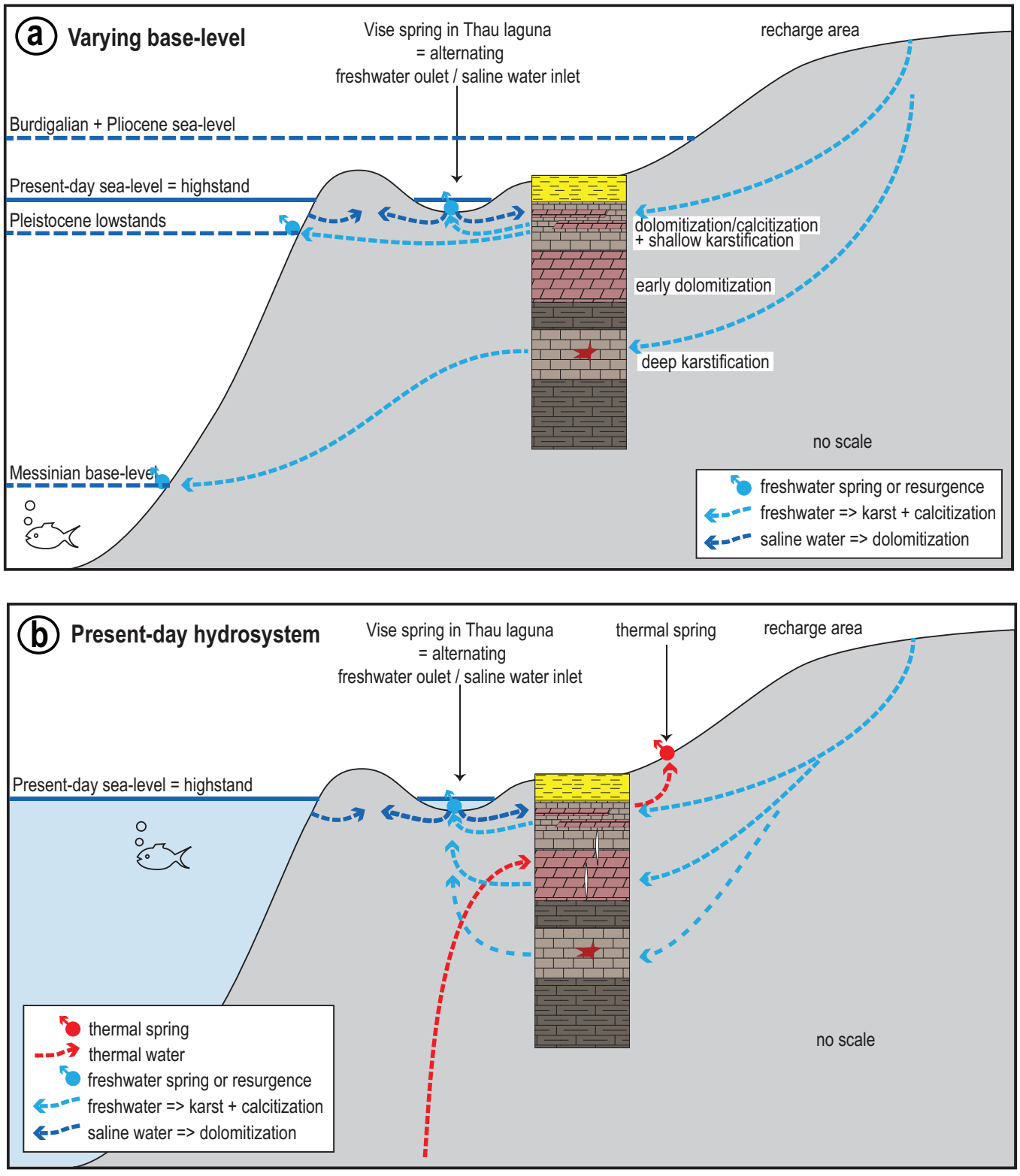

Fig. 15. a: conceptual model of alternating fresh and saline water circulation in the upper reservoir, responsible for successive episodes of dolomitization and calcitization of the carbonates. The lithological section in the centre corresponds to the studied borehole (same color code as for Fig. 3). Alternance of water circulation through the Vise spring in the Thau laguna and in the underlying reservoir could be tuned to the "inversac" phenomenon or (more likely), to longer period processes such as glacio-eustacy during Pleistocene, or regional tectonically-driven sea-level changes. See text for explanations; b: present-day setting of the Balaruc hydrosystem in relation with the architecture of the reservoir. The karstic waters circulate preferentially in the upper reservoir and through subvertical open crack in the dolomite reservoir; minor flows are recorded in the very deep reservoir. Upward flow of thermal water circulates across the dolomite reservoir through the same subvertical cracks and reaches surface level at natural thermal springs.

and deep thermal water, each with important economic and social stakes. Hydrological modelling of this hydrosystem requires an improved knowledge of the reservoir, which has been addressed by drilling an exploratory 750 m deep borehole entirely cored. Preliminary analyses of the cores, specifically of the small-scale structures, of the karst fillings and of the calcite mineralizations has led to the following observations:

- the carbonate reservoir consists of Jurassic limestones covered by Neogene marls. Limestones have been subjected to two distinct types of dolomitization: (i) an early dolomitization of mudstones affected a lower reservoir, prior to a phase of pervasive cataclastic deformation and (ii) a Neogene to possibly Present dolomitization partially affected grainstones of the shallow reservoir;
- cross-cutting relationships of the structures and of the associated calcite mineralization allowed to establish a relative chronology, which can be correlated with the regional geodynamic evolution. Following the compaction-related subhorizontal stylolites and associated vertical calcite veins, the major deformation stage of the reservoir corresponds to a late Early-Cretaceous NNE–SSW extensional event related to the "Durancian uplift", overprinted by NS compression related to the Pyrenean event expressed by sub-vertical tension gashes. The basin-scale geometry was finally acquired during the Oligocene-Aquitanian rifting of the Gulf of Lion;
- the study of calcite mineralization and chemical alterations of the reservoir shows similarities between the paleofluids that circulated through the reservoir and current fluids of the present hydrosystem. However, it is most unlikely that the latter is older than the Pliocene cover of the reservoir;
- dolomitization of the upper reservoir by Mg-rich seawater is favoured by alternate circulation of: (i) karstic freshwaters that create and develop a dense network of conduits as well as drastically increasing the contact surface for fluid-rock interaction and (ii) marine salty waters that penetrate deeply in the reservoir, using the karstic network;
- 450–500 m-deep paleo-karst filled with continental silts witness fluxes of meteoric corrosive water, driven by an even deeper outlet. Regional geodynamics suggests Paleocene and/or Messinian ages;
- the up-flowing geothermal water circulates across the lower dolomite reservoir through the Thau thrust, an inherited Pyrenean structure.

Our study indicates that the long-term geodynamic evolution has shaped the Jurassic karstic reservoir of the Balaruc peninsula, while the lithostratigraphic structures and deformation facies controlled the texture of this reservoir, and organised the connections within the current hydrogeological system. Although the present-day hydrosystem reactivates structures inherited from the long-term geodynamic evolution, it is subjected to turn-overs on a much faster rate, driven by high-frequency external forcings such as sea-level changes driven by Pleistocene glacio-eustasy, or climate changes controlling varying amounts of precipitation. Under the effects of the current climate change, the expected sea-level rise combined with aridification may raise concern for the future of the studied hydrosystem.

Further ongoing geochemical studies of the mineralizations will help constraining sources, residence time, paleo-temperatures of paleo-fluids interacting with the host-rocks.

Acknowledgements. This work is part of the Dem'Eaux Thau Project, funded by: European Community, French State, Région Occitanie, Agence de l'eau RMC, SMBT, City of Balaruc-les-Bains, and Montpellier Méditerranée Métropole. We are grateful to GeoSonic and Hydroforage companies who skillfully operated drilling and core recovery, as well as to Vincent Durand of Antea for managing the operations. Thanks are due to Christophe Nevado and Doriane Delmas for the quality thin sections they provided. The work benefited from discussions amongst the Dem'Eaux Thau working group within BRGM, Géosciences Montpellier and HydroSciences Montpellier. The manuscript has been improved by thoughtful reviews of Benoit Vincent and of an anonymous reviewer.

References

Allmendinger RW, Cardozo NC, Fisher D. 2012. Structural geology algorithms: vectors & tensors. Cambridge, England: Cambridge University Press, 289 p.

Ambert P, Aguilar JP, Michaux J. 1998. Évolution géodynamique messino-pliocène en Languedoc central : le paléo-réseau hydrographique de l'Orb et de l'Hérault (Sud de la France). *Geodinamica Acta* 11: 139–146.

Aquilina L, Ladouche B, Doerfliger N, Seidel J-L., Bakalowicz M, Dupuy C, *et al.* 2002. Origin, evolution and residence time of saline thermal fluids (Balaruc springs, southern France): implications for fluid transfer across the continental shelf. *Chemical Geology* 192: 1–21.

Aquilina L, Ladouche B, Doerfliger N, Bakalowicz M. 2003. Deep water circulation, residence time, and chemistry in a karst complex. *Ground Water* 41: 790–805.

Arfib B, Gilli E. 2010. Karst côtier et sources sous-marines. Fonctionnement et exploitation. In: Audra P, ed. Grottes et karsts de France. Karstologia Mémoires n° 19. Association française de karstologie, pp. 128–129.

Arthaud F, Séguret M. 1981. Les structures pyrénéennes du Languedoc et du Golfe du Lion (Sud de la France). *Bulletin de la Société géologique de France* XXIII: 51–63.

Arthaud F, Laurent P. 1995. Contraintes, déformation et déplacement dans l'avant-pays Nord-pyrénéen du Languedoc méditerranéen. *Geodynamica Acta* 8: 142–157.

Audra P, Mocochain L, Camus H, Gilli E, Clauzon G, Bigot J-Y. 2004. The effect of the Messinian deep-stage on karst development around the Mediterranean Sea. Examples from southern France. *Geodinamica Acta* 17: 389–400.

Barbarand J, Lucazeau F, Pagel M, Séranne M. 2001. Burial and exhumation history of the south-eastern Massif Central (France) constrained by an apatite fission-track thermochronology. *Tectonophysics* 335: 275–290.

Beaudoin N, Lacombe O, Roberts NMW, Koehn D. 2018. U-Pb dating of calcite veins reveals complex stress evolution and thrust sequence in the Bighorn Basin, Wyoming, USA. *Geology* 46: 1015–1018.

Benedicto A, Labaume P, Séguret M, Séranne M. 1996. Low-angle crustal ramp and basin geometry in the Gulf of Lion passive margin: the Oligocene-Aquitanian Vistrenque graben, SE France. *Tectonics* 15: 1192–1212.

Benedicto A, Séguret M, Labaume P. 1999. Interaction between faulting, drainage and sedimentation in extensional hanging-wall

syncline basins: example of the Oligocene Matelles Basin, Gulf of Lion margin (S.E. France). In: Durand B, Jolivet L, Horváth F, Séranne M, eds. The Mediterranean Basins: tertiary extension within the Alpine Orogen. Special Publication 156. London: The Geological Society, pp. 81–108.

Benjakul R, Hollis C, Robertson HA, Sonnenthal EL, Whitaker FF. 2020. Understanding controls on hydrothermal dolomitisation: insights from 3D reactive transport modelling of geothermal convection. *Solid Earth* 11: 2439–2461.

Bérard P. 1995. Le bassin de Thau (Hérault) – Synthèse des connaissances géologiques et hydrogéologiques. BRGM. Rapport R38538, 94 p.

Bicalho CC, Batiot-Guilhe C, Taupin JD, Patris N, Van Exter S, Jourde H. 2019. A conceptual model for groundwater circulation using isotopes and geochemical tracers coupled with hydrodynamics: a case study of the Lez karst system, France. *Chemical Geology* 528: 118442.

Bruxelles L. 2001. Dépôts et altérites des plateaux du Larzac central : Causses de l'Hospitalet et de Campestre (Aveyron, Gard, Hérault) – Évolution morphogénétique, conséquences géologiques et implications pour l'aménagement. Doctorat, Univ. Aix-Marseille 1, 245 p.

Bussolotto M, Benedicto A, Moen-Maurel L, Invernizzi C. 2015. Fault deformation mechanisms and fault rocks in micritic limestones: examples from Corinth rift normal faults. *Journal of Structural Geology* 77: 191–212.

Cantarero I, Travé A, Alías G, Baqués V. 2013. Polyphasic hydrothermal and meteoric fluid regimes during the growth of a segmented fault involving crystalline and carbonate rocks (Barcelona Plain, NE Spain). *Geofluids* 14: 20–44.

Célérier B, Etchecopar A, Bergerat F, Vergely P, Arthaud F, Laurent P. 2012. Inferring stress from faulting: from early concepts to inverse methods. *Tectonophysics* 581: 206–219.

Chanvry E, Marchand E, Lopez M, Séranne M, Le-Sout G, Vinches M. 2020. Tectonic and climate control on allochthonous bauxite deposition. Example from the mid-Cretaceous Villeveyrac basin, southern France. *Sedimentary Geology* 407.

Chauvet A. 2019. Structural control of ore deposits: the role of pre-existing structures on the formation of mineralised vein syste. *Minerals* 9: 56.

Clauzon G. 1973. The eustatic hypothesis and the pre-Pliocene cutting of the Rhône valley. In: Hsü KJ, Cita MB, Ryan WBF, eds. Initial Repts of Deep Sea Drilling Project. Washington: 13: US Gov. Printing Office, pp. 1251–1256.

Clauzon G. 1982. Le canyon messinien du Rhône : une preuve décisive du « dessicated deep-basin model » (Hsü, Cita et Ryan, 1973). *Bulletin de la Société géologique de France* 24: 597–610.

Combes P-J. 1990. Typologie, cadre géodynamique et genèse des bauxites françaises. *Geodinamica Acta* 2: 91–109.

Combes P-J., Peybernès B, Fondecave-Wallez M-J., Séranne M, Lesage J-L., Camus H. 2007. Latest-Cretaceous/Paleocene karsts with marine infillings from Languedoc (South of France); paleogeographic, hydrogeologic and geodynamic implications. *Geodinamica Acta* 20: 301–326.

Coniglio M. 2003. Dedolomitization. In: Middleton GV, ed. Encyclopedia of Sediments and Sedimentary Rocks – Encyclopedia of Earth Sciences Series. Springer, pp. 188–190.

Davies GR, Smith LB. 2006. Structurally controlled hydrothermal dolomite reservoir facies: an overview. *AAPG Bulletin* 90: 1641–1690.

de Montety V, Radakovitch O, Vallet-Coulom C, Blavoux B, Hermitte D, Valles V. 2008. Origin of groundwater salinity and hydrogeochemical processes in a confined coastal aquifer: case of the Rhône delta (Southern France). *Applied Geochemistry* 23: 2337–2349.

Debrand-Passard S, Courbouleix S. 1984. Synthèse géologique du Sud-Est de la France – Stratigraphie et paléogéographie. Orléans, France: BRGM, 615 p.

Dörfliger N, Fleury P, Le Strat P, Capar L. 2008. Caractérisation géologique et hydrogéologique des aquifères carbonates karstiques sous couverture. Méthodologie, synthèse bibliographique et synthèse géologique régionale. BRGM. Rapport final BRGM-RP-56980-FR, 157 p.

Drogue C, Bidaux P. 1986. Simultaneous outflow of fresh water and inflow of seawater in a coastal spring. *Nature* 322: 361–363.

Duretz T, Asti R, Lagabrielle Y, Brun JP, Jourdon A, Clerc C, *et al.* 2020. Numerical modelling of Cretaceous Pyrenean Rifting: the interaction between mantle exhumation and syn-rift salt tectonics. *Basin Research* 34: 652–667.

Fleury P, Bakalowicz M, De Marsily G. 2007. Submarine springs and coastal karst aquifers: a review. *Journal of Hydrology* 339: 79–92.

Fournier F, Tassy A, Thinon I, Münch P, Cornée J-J., Borgomano J, *et al.* 2016. Pre-Pliocene tectonostratigraphic framework of the Provence continental shelf (eastern Gulf of Lion, SE France). *Bulletin de la Société géologique de France* 187: 187–216.

Fuchey Y, Le Strat P, Bourgine B. 2001. Atlas des cartes isohypses et isopaques des formations Plio-Quaternaires de la vallée de l'Hérault. BRGM. RP-50770-FR, 42 p.

Gaillot P, Maria-Sube Y, Pezard PA. 2005. Quantification of meso-scale porosity from borehole wall images: a comparative study – Example from the ALIANCE Campos experimental site, Mallorca, Spain. In: 11th Formation Evaluation Symposium of Japan.

Gaillot P, Brewer T, Pezard P, Yeh E-C. 2007. Contribution of borehole digital imagery in core-log-seismic integration. *Scientific Drilling* 5: 50–53.

Gèze B. 1987. Les mésaventures des sources de l'Estavelle et de l'Inversac en languedoc Méditerranéen. *International Journal of Speleology* 16: 101–109.

Gignoux M. 1926. Géologie stratigraphique. Paris: Masson & Cie, 588 p.

Gilli E. 2020. A Messinian model explains the salt contamination of the Mediterranean Coastal Springs. *Environmental Earth Sciences* 79: 188.

Gottis M, Denizot G, Combes P-J., Bertrand JM, Seguret M, Gérard M, *et al.* 1967. Carte géologique de la France au 1/50 000. Feuille de Sète n° 1016. BRGM.

Gratier JP, Renard F, Labaume P. 1999. How pressure solution and fracturing processes interact in the upper crust to make it behave in both a brittle and viscous manner. *Journal of Structural Geology* 21: 1189–1197.

Hansman RJ, Albert R, Gerdes A, Ring U. 2018. Absolute dating of multiple generation of brittle structures ny U-Pb dating of calcite. *Geology* 46: 207–210.

Hausegger S, Kurz W, Rabitsch R, Kiechl E, Brosch F-J. 2010. Analysis of the internal structure of a carbonate damage zone: implications for the mechanisms of fault breccia formation and fluid flow. *Journal of Structural Geology* 32: 1349–1362.

Hemelsdaël R, Séranne M, Caritg S, Courrioux G, Husson E, Jacob T, *et al.* 2021a. Dem'Eaux Thau – Construction d'un modèle géologique 3D du secteur Montpellier-Sète et de l'étang de Thau. BRGM. RP-70789-FR, 94 p.

Hemelsdaël R, Séranne M, Husson E, Ballas G. 2021b. Structural style of the Languedoc Pyrenean thrust belt in relation with the inherited Mesozoic structures and with the rifting of the Gulf of Lion margin, southern France. *BSGF-Earth Sciences Bulletin* 192: 46.

Husson E, Séranne M, Combes P-J., Camus H, Peybernès B, Fondecave-Wallez M-J, *et al.* 2012. Marine karstic infillings: witnesses of extreme base level changes and geodynamic consequences (Paleocene of Languedoc south of France). *Bulletin de la Société géologique de France* 183: 425–441.

Husson E. 2013. Interaction géodynamique/karstification et modélisation géologique 3D des massifs carbonatés : implication sur la distribution prévisionnelle de la karstification. Exemple des paléokarsts crétacés à néogènes du Languedoc montpelliérain. Doctorat, Université Montpellier 2, 314 p.

Husson E, Guillen A, Séranne M, Courrioux G, Couëffé R. 2018. 3D geological modeling and gravity inversion of a structurally complex carbonate area: application for karstified massif localization. *Basin Research* 30: 766–782.

Jébrak M. 1997. Hydrothermal breccias in vein-type ore deposits: a review of mechanisms, morphology and size distribution. *Ore Geology Reviews* 12: 11–134.

Kaczmarek S, Thornton B. 2017. The effect of temperature on stoichiometry, cation ordering, and reaction rate in high-temperature dolomitization experiments. *Chemical Geology* 468: 32–41.

Khaska M, La Salle CL, Lancelot J, Mohamad A, Verdoux P, Noret A, *et al.* 2013. Origin of groundwater salinity (current seawater vs. saline deep water) in a coastal karst aquifer based on Sr and Cl isotopes. Case study of the La Clape massif (southern France). *Applied Geochemistry* 37: 212–227.

Khaska M, Salle CLGL, Videau G, Flinois J-S., Frape S, Team A, *et al.* 2015. Deep water circulation at the northern Pyrenean thrust: Implication of high temperature water-rock interaction process on the mineralization of major spring water in an overthrust area. *Chemical Geology* 419: 114–131.

Labaume P, Carrio-Schaffhauser E, Gamond J-F., Renard F. 2004. Deformation mechanisms and fluid-driven mass transfers in the recent fault zones of the Corinth Rift (Greece). *Comptes rendus géosciences* 336: 375–383.

Ladouche B, Bakalowicz M, Courtois N, Dörfliger N, Pinault J-L., Chemin P, *et al.* 2001. Étude du pourtour de l'étang de Thau (Hérault) – phase II – Fonctionnement hydrogéologique du bassin karstique de Thau, volume 2. BRGM. BRGM/RP-50787-FR, 275 p.

Ladouche B, Lamotte C, Hemelsdaël R, Pétré M-A., Dewandel B, Léonardi V, *et al.* 2019. DEM'EAUX Thau – Synthèse et valorisation préliminaire des données sur l'hydrosystème de Thau (34) – Rapport final. BRGM. BRGM/RP-68483-FR, 313 p.

Ladouche B, Lamotte C, Séranne M. 2021. Interactions de fluides (eaux douces, marines, thermales) dans les réservoirs karstiques sous couverture de la marge proximale du Golfe du Lion : le projet DEM'EAUX Thau. 27^{e} RST. Lyon: Société géologique de France.

Ladouche B, Séranne M, De Montety V, Ranchoux C, Dewandel B, Hakoun V, *et al.* 2022. DEM'Eaux Thau : rapport de synthèse final. BRGM. BRGM/RP-77471-FR, 129 p.

Lagabrielle Y, Labaume P, De Saint Blanquat M. 2010. Mantle exhumation, crustal denudation, and gravity tectonics during Cretaceous rifting in the Pyrenean realm (SW Europe): insights from the geological setting of the lherzolite bodies. *Tectonics* 29 (TC4012): 4011–4026.

Lajoinie J-P, Laville P. 1979. Les formations bauxitiques de la Provence et du Languedoc. Dimensions et distribution des gisements. *Mémoire du BRGM* 100: 146.

Lamotte C. 2019. Projet DEM'Eaux-Thau-Instrumentation de la source de la Vise à Balaruc-les-Bains (34) – Rapport de fin de travaux-Livrable L7–Rapport final. BRGM. BRGM/RP-69163-FR, 23 p.

Laurent D. 2015. Marqueurs de la dynamique des fluides associée à l'enfouissement des bassins sédimentaires : exemples du Bassin Permien de Lodève (France) et du North Viking Graben (Mer du Nord). Doctorat, Université de Montpellier, 597 p.

Lofi J, Deverchère J, Gaullier V, Gillet H, Gorini C, Guennoc P, *et al.* 2011. Seismic Atlas of the "Messinian Salinity Crisis" Markers in the Mediterranean and Black Seas. Paris: Commission for the Geological Map of the World and Mémoires de la Société géologique de France, 179, 79 p.

Lofi J, Berné S, Tesson M, Séranne M, Pezard P. 2012. Giant solution-subsidence structure in the Western Mediterranean related to deep substratum dissolution. *Terra Nova* 24: 181–188. https://doi.org/110.1111/j.1365-3121.2011.01051.x.

Machel HG. 2000. Application of cathodoluminescence to carbonate diagenesis. In: Pagel M, Barbin V, Blanc P, Ohnenstetter D, eds. Cathodoluminescence in Geosciences. Bert, Heidelberg, New York: Springer, pp. 271–302.

Machel HG. 2004. Concepts and models of dolomitization: a critical reappraisal. In: Braithwaite CJR, Rizzi G, Darke G, eds. The geometry and petrogenesis of dolomite hydrocarbon reservoirs, Special Publications 235. London: Geological Society, pp. 7–63.

Machel HG, Lonnee J. 2002. Hydrothermal dolomite—a product of poor definition and imagination. *Sedimentary Geology* 152: 163–171.

Marchand E. 2019. Rôle des interactions tectonique-sédimentation sur l'évolution et la variabilité spatiale d'un gisement de bauxite karstique : exemple du bassin de Villeveyrac (sud de la France). Doctorat, Université de Montpellier – IMT Mines Alès, 303 p.

Marchand E, Séranne M, Bruguier O, Vinches M. 2020. LA-ICP-MS dating of detrital zircon grains from the Cretaceous allochthonous bauxites of Languedoc (south of France): provenance and geodynamic consequences. *Basin Research* 33: 270–290.

Meyers WJ. 1991. Calcite cement stratigraphy: an overview. In: Barker CE, Burruss RC, Kopp OC, Machel HG, Marshall DJ, Wright P, Colbum HY, eds. Luminescence microscopy and spectroscopy: qualitative and quantitative applications, SEPM Short Course Notes 25. SEPM, pp. 133–148.

Milodowski AE, Bath A, Norris S. 2018. Palaeohydrogeology using geochemical, isotopic and mineralogical analyses: Salinity and redox evolution in a deep groundwater system through quaternary glacial cycles. *Applied Geochemistry* 97: 40–60.

Moss SJ, Tucker ME. 1996. Dolomitization associated with transgressive surfaces— a mid-Cretaceous example. *Sedimentary Geology* 107: 11–20.

Pagel M, Bonifacie M, Schneider DA, Gautheron C, Brigaud B, Calmels D, *et al.* 2018. Improving paleohydrological and diagenetic reconstructions in calcite veins and breccia of a sedimentary basin by combining Delta(47) temperature, delta O-18 (water) and U-Pb age. *Chemical Geology* 481: 1–17.

Parizot O. 2021. Expression et âge de la déformation intraplaque au front d'un orogène : du Chevauchement Frontal Nord-Pyrénéen à la bordure Sud du Massif Central, France. Doctorat, Paris-Saclay, 371 p.

Parizot O, Missenard Y, Haurine F, Blaise T, Barbarand J, Benedicto A, *et al.* 2021. When did the Pyrenean shortening end? Insight from U-Pb geochronology of syn-faulting calcite (Corbières area, France). *Terra Nova* 00: 1–9.

Petelet-Giraud E, Negrel P, Aunay B, Ladouche B, Bailly-Comte V, Guerrot C, *et al.* 2016. Coastal groundwater salinization: focus on the vertical variability in a multi-layered aquifer through a multi-isotope fingerprinting (Roussillon Basin, France). *Science of the Total Environment* 566: 398–415.

Pétré M-A., Ladouche B, Seidel J-L., Hemelsdaël R, de Montety V, Batiot-Guilhe C, *et al.* 2020. Hydraulic and geochemical impact of occasional saltwater intrusions through a submarine spring in a karst and thermal aquifer (Balaruc peninsula near Montpellier, France). *Hydrology and Earth System Sciences* 24: 5656–5672.

Petrini R, Italiano F, Ponton M, Slejko FF, Aviani U, Zini L. 2013. Geochemistry and isotope geochemistry of the Monfalcone thermal waters (northern Italy): inference on the deep geothermal reservoir. *Hydrogeology Journal* 21: 1275–1287.

Pinault J-L., Dörfliger N, Ladouche B, Bakalowicz M. 2004. Characterizing a coastal karst aquifer using an inverse modeling approach. The saline springs of Thau, Southern France. *Water Resources Research* 40: W08501.

Rabineau M, Berné S, Aslanian D, Olivet J-L., Joseph P, Guillocheau F, *et al.* 2005. Sedimentary sequences in the Gulf of Lion: a record of 100,000 years climatic cycles. *Marine and Petroleum Geology* 22: 775–804.

Radwan OA, Dogan AU, Morsy MA, Kaminski MA, Humphrey JD, Christiansen EH. 2021. One-step versus two-step dolomite calcitization (dedolomitization): differences and inferences. *Geosciences Journal* 25: 453–464.

Ranchoux C, Ladouche B, Montety De V, Seidel J-L, Pétré MA, Hery M, *et al.* 2022. DEM'Eaux Thau- Rapport d'analyses géochimiques – Apport des campagnes spatiales 2018–2019 - Livrable L5a. Rapport final. BRGM, 153 p.

Richter DK, Götte T, Götze J, Neuser RD. 2003. Progress in application of cathodoluminescence (CL) in sedimentary geology. *Mineralogy and Petrology* 79: 127–166.

Rispoli R. 1981. Stress fields about strike-slip faults inferred from stylolites and tension gashes. *Tectonophysics* 75: 29–36.

Roberts NMW, Walker RJ. 2016. U-Pb geochronology of calcite-mineralized faults: absolute timing of rift-related fault events on the northeast Atlantic margin. *Geology* 44: 531–534.

Séranne M. 1999. The Gulf of Lion continental margin (NW Mediterranean) revisited by IBS: an overview. In: Durand B, Jolivet L, Horváth F, Séranne M, eds. The Mediterranean Basins: tertiary extension within the Alpine Orogen, Special Publication 156. London: The Geological Society, pp. 15–36.

Séranne M, Camus H, Lucazeau F, Barbarand J, Quinif Y. 2002. Surrection et érosion polyphasées de la bordure cévenole – Un exemple de morphogenèse lente. *Bulletin de la Société géologique de France* 173: 97–112.

Sibson RH. 1977. Fault rocks and fault mechanisms. *Journal of the Geological Society* 133: 191–213.

Soreghan GS, Engel MH, Furley RA, Giles KA. 2000. Glacioeustatic transgressive reflux: Stratiform dolomite in Pennsylvanian bioherms of the Western Orogrande Basin, New Mexico. *Journal of Sedimentary Research* 70: 1315–1332.

Stacey J, Hollis C, Corlett H, Koeshidayatullah A. 2020. Burial dolomitization driven by modified seawater and basal aquifer-sourced brines: insights from the Middle and Upper Devonian of the Western Canadian Sedimentary Basin. *Basin Research* 33: 648–680.

Tavani S, Bertok C, Granado P, Piana F, Salas R, Vigna B, *et al.* 2018. The Iberia-Eurasia plate boundary east of the Pyrenees. *Earth-Science Reviews* 187: 314–337.

Torabi A, Berg SS. 2011. Scaling of fault attributes: a review. *Marine and Petroleum Geology* 28: 1444–1460.

Toussaint R, Aharonov E, Koehn D, Gratier J, Ebner M, Baud P, *et al.* 2018. Stylolites: a review. *Journal of Structural Geology* 114: 163–195.

Travé A, Labaume P, Vergés J. 2007. Fluid Systems in Foreland Fold-and-Thrust Belts: An Overview from the Southern Pyrenees. In: Lacombe O, Roure F, Lavé J, Vergés J, eds. Thrust Belts and Foreland Basins. Frontiers in Earth Sciences. Berlin, Heildeberg: Springer, pp. 93–115.

Travé A, Rodriguez-Morillas N, Baques V, Playa E, Casas L, Cantarero I, *et al.* 2021. Origin of the Coloured Karst Fills in the Neogene Extensional System of NE Iberia (Spain). *Minerals* 11: 1382.

Vahrenkamp VC, Swart PK. 1994. Late Cenozoic dolomites of the Bahamas: metastable analogues for the genesis of ancient platform dolomites. In: Purser B, Tucker M, Zenger D, eds. Dolomites: a volume in honour of Dolomieu. Special Publication 21. International Association of Sedimentologists, pp. 133–153.

Yang P, Liu KY, Li Z, Rankenburg K, Mcinnes BIA, Liu JL, *et al.* 2022. Direct dating Paleo-fluid flow events in sedimentary basins. *Chemical Geology* 588.

Cite this article as: Widhen F, Séranne M, Ballas G, Labaume P, Le-Ber E, Pezard P, Girard F, Lamotte C, Ladouche B. 2023. Long-term evolution of a carbonate reservoir submitted to fresh, saline and thermal waters interactions – Jurassic carbonates in the coastal area of the Gulf of Lion margin (southern France), *BSGF - Earth Sciences Bulletin* 194: 7.